DEPARTMENT OF MEDICINE

TECHNISCHE UNIVERSITÄT MÜNCHEN

Master's Thesis in Neuroengineering

Identifying Alterations in Effective Connectivity and Fractional Anisotropy in Patients with Early Psychosis using BOLD fMRI and dMRI

Corey Jones

DEPARTMENT OF MEDICINE

TECHNISCHE UNIVERSITÄT MÜNCHEN

Master's Thesis in Neuroengineering

Identifying Alterations in Effective Connectivity and Fractional Anisotropy in Patients with Early Psychosis using BOLD fMRI and dMRI

Author:	Corey Jones
Supervisor:	Afra Wohlschläger
Advisor:	Afra Wohlschläger
Submission Date:	25.09.2023

I confirm that this master's thesis in neuroengineering is my own work and I have documented all sources and material used.

Munich, 25.09.2023 Corey Jones

Abstract

This thesis investigates alterations in effective connectivity and fractional anisotropy related to early psychosis. Resting state BOLD fMRI data are used to generate spectral dynamic causal models using information from two distinct frequency bands, namely slow 5 (0.01 - 0.027Hz) and slow 4 (0.027 - 0.073Hz). Those models are refined using parametric empirical bayesian methods and bayesian model reduction to generate reliable estimates of effective connectivity within and between the nodes of the default mode network, control executive network, and salience network. Diffusion MRI data are used to generate fractional anisotropy estimates, that are used to compare white matter densities between the patient and control groups at various regions distributed throughout the brain. The effective connectivity values are correlated with disease severity by means of canonical variate analysis. The results of this thesis are that there are alterations in effective connectivity and regional average fractional anisotropies that are generally consolidated within the prefrontal, parietal, temporal, and sub-cortical nuclei, which is consistent with findings published in the literature. Additionally, this study finds that the effective connections that most strongly explain variance in disease severity are generally among those that exhibit either significantly altered effective connectivity profiles, fractional anisotropy values, or both. Overall, this study corroborates findings of other studies with similar research questions and provides novel information given that it uses fully connected multi-network models using a relatively large number of subjects (57 patients and 39 controls) and that it separates models into two distinct frequency bands. In future studies, classification algorithms will be trained to identify the risk a given individual has of developing early psychosis based on these neuroimaging metrics, and the possible mediating role of fractional anisotropy on the relationship between effective connectivity and disease severity will be isolated and investigated.

Contents

1. Introduction

The purpose of this study is to investigate the neuroanatomical and neurophysiological underpinnings of psychosis as it relates to schizophrenia spectrum disorders. Generally, people with schizophrenia spectrum disorders exhibit either positive or negative clinical symptoms, or both, that consist of features such as delusions and hallucinations or anhedonia and avolition, respectively. A paper by Tahir Rahman and John Lauriello titled "Schizophrenia: An overview" was published in 2016 and provides a good, concise summary of what the epidemiology and clinical definitions of schizophrenia are and how it can present differently from person to person [57]. In 2015, an article titled "Psychosis" was published by David B. Arciniegas (MD), that provides good definitions of the features of psychosis and how it relates to schizophrenia spectrum disorders [5]. This thesis does not present a systematic review of the literature pertaining to the neural mechanisms that have been implicated in the onset and development of schizophrenia. However, a selection of studies will be referred to throughout the text to describe some of the modern methods used to evaluate alterations in neuroanatomy and physiological activity found to be common among patients with schizophrenic spectrum disorders; specifically, these references will mostly pertain to methods and findings from studies using Blood Oxygen Level Dependent (BOLD) Functional Magnetic Resonance Imaging (fMRI) and Diffusion Weighted Image (DWI) data, as those are the data types that are used in this study. Technical definitions for terms with corresponding acronyms are available in the Glossary, and if the reader is using the interactive pdf, then it is possible to be directed to the respective definition by clicking on the word, phrase, or acronym.

This study specifically aims to identify the most salient differences in Effective Connectivity (EC) between healthy controls and patients with schizophrenia spectrum disorders within three major brain networks, that may implicate altered region to region interactions in the brain that lead to the development of schizophrenia and its corresponding symptoms. The study also aims to identify differences in regional average Fractional Anisotropy (FA) to assess where and how differences in white matter density can predict alterations in EC and in disease severity. The final goal of this study is to evaluate whether the modeled EC values can explain a substantial degree of variance in features corresponding to disease severity. To answer these questions, neuroimaging data from 169 subjects were used and 21 Regions of Interest (ROIs) spanning the Default Mode network (DMN), Control Executive network (CEN), and Salience network (SN) were included in a series of fully connected Spectral Dynamic Causal Models (spDCMs) [26]. Details about where the subject data were acquired and what types of neuroimaging data were used are provided in the following section, and in the subsequent section details pertaining to the included nodes and brain networks are described. Descriptions about what spDCMs are and where the method originated are provided in the

methods in section 2.2.

1.1. Subject Information & Image Acquisition Details

Data were provided by the Human Connectome Project for Early Psychosis (HCP-EP). Data were made available for 79 patients meeting "DSM-V diagnosis criteria for schizophrenia, schizophreniform disorder, schizoaffective disorder, psychosis not otherwise specified, delusional disorder, or brief psychosis disorder with onset within five years prior to study entry"[1]. The healthy control group consists of 54 subjects. Full details of inclusion and exclusion criteria for each subject group are available on pages 4-6 in the release notes for the data set at the link below[1]. In the data release, each of these subjects has $2mm^3$ isotropic resting state BOLD fMRI data that were collected in two phase encoding directions (AP and PA in separate scans) at a Repetition Time (TR) of 800ms. Each session consisted of 410 scans, thus taking a total of 328 seconds each. The Diffusion weighted image data provided have an isotropic resolution of $1.5mm^3$; the release notes state that "92 directions were measured in each shell (b=1500 and 3000) acquired twice: once with AP and once with PA phase encoding. The first two acquisitions include 3 additional directions at b=200 and 6 directions at b=500 to improve modeling of fast diffusion processes such as free water"[1]. All methods and analyses in this study were produced using the data that were collected in the PA encoding direction. Complete details about the scanning procedures are documented in Appendix 1 of the HCP-EP release notes[2]; the descriptions for the resting state fMRI and dMRI data that were used in this study are listed on pages 20 and 28 of that appendix, respectively.

1.1.1. Demographics

The demographics table (Figure 1.1) shows the compositions of each group by sex, age, and mother's education level. It also indicates mean scores on an array of cognitive assessments, and for the patient group indicates mean symptom severity across Positive and Negative Syndrome Scale (PANSS) dimensions. As indicated by the P-val column, there is a statistically significant difference in the mean age between the groups, where the controls are approximately three years older than the patients on average. There is also a statistically significant difference in the median mother's education level between the groups (control median = 6, patient median = 5), indicating that the median education of the mother's of the subjects of the control group was "Completed 7^{th} through 9^{th} grades" and for the patients was "Completed 10^{th} through 11^{th} grades". In this table, it is also clear that the schizophrenic group performs statistically significantly worse on average across a variety of cognitive scores.

Tests with more than one degree of freedom indicate that a two-sided t-test was used to test for differences in means of the respective scores between the groups via the **ttest_ind** function

[1] https://www.humanconnectome.org/storage/app/media/documentation/data_release/HCP-EP_Release_1.0_Manual.pdf

[2] https://www.humanconnectome.org/storage/app/media/documentation/data_release/Appendix%201_HCP-EP_Release_Imaging_Protocols.pdf

LABELS	CONTROLS	PATIENTS	P-VAL	DF
Sex (M/F)	28/11	45/12	0.573474	1
Age (Years)	24.902 ± 7.860	22.060 ± 6.434	0.000192	94
Mother's Education	5.92 ± 1.94	5.11 ± 2.53	0.002395	1
Auditory RT	622.00 ± 146.72 (ms)	665.52 ± 220.47 (ms)	0.038856	88
Auditory HR	91.14 ± 11.09	76.89 ± 33.78	0.000003	91
Fluid Cognition	111.89 ± 18.65	95.87 ± 30.77	0.000000	89
Crystallized Cognition	110.16 ± 14.85	99.51 ± 20.13	0.000000	91
Emotion Recognition (RT)	1694.25 ± 518.15 (ms)	2368.78 ± 2076.27 (ms)	0.000525	86
Emotion Recognition (CR)	36.03 ± 3.95	32.80 ± 10.01	0.000770	86
Wasi IQ	113.97 ± 10.81	97.14 ± 16.86	0.000000	93
PANSS Positive	-	13.33 ± 11.30	-	-
PANSS Negative	-	11.49 ± 9.35	-	-
PANSS Total	-	50.31 ± 25.08	-	-
PANSS General	-	25.49 ± 13.93	-	-

Figure 1.1.: Demographic information about the control and patient groups with p-values and degrees of freedom from difference in mean and median tests for select cognitive scores, age, sex, and mother's education

in the scipy.stats Python module. The difference in proportion of males and females between the groups was tested using a Chi square test for independence via the **chi2_contingency** function in the scipy.stats Python module. The difference in mother's education test statistic was generated using a the Mann-Whitney-Wilcoxon test implemented via the **mannwhitneyu** function in the scipy.stats Python module. More detailed attention will be given to the differences in mean cognitive scores between the groups in the results (section 3.5).

1.2. Network and ROI selection

The regions of interest (ROIs) selected for this study were based upon existing works, specifically Razi et al., 2017 [61], who use a set of ROIs from Raichle's 2011 article "The restless brain" [59]. I chose a subset of ROIs from the 36 presented in the Razi publication, specifically choosing the nodes comprising the Default Mode network (DMN), Control Executive network (CEN), and Salience network (SN). These three networks are comprised of 21 nodes in total, and notably make up the "triple network", that has been implicated in a wide range of neurological and psychiatric disorders [51]. To avoid spillover effects of neighboring regions being modeled, the sizes of the ROIs were scaled by the anatomical depth of the region.

The size, position (in mm using MNI coordinates), and network belongingness of each ROI is represented in Table 1.1. Full names of each node's abbreviated label are listed in the Glossary.

Table 1.1.: ROI labels, positions, diameters, and network belongingness as shown in Razi et al., 2017 [61]

Labels	x	y	z	Radius	Network
PCC	0	-52	7	6*mm*	DMN
mPFC	-1	54	27	8*mm*	DMN
LlPar	-46	-66	30	8*mm*	DMN
RlPar	49	-63	33	8*mm*	DMN
LiTem	-61	-24	-9	8*mm*	DMN
RiTem	58	-24	-9	8*mm*	DMN
mdThal	0	-12	9	6*mm*	DMN
LpCerb	-25	-81	-33	4*mm*	DMN
RpCerb	25	-81	-33	4*mm*	DMN
dmPFC	0	24	46	8*mm*	CEN
LaPFC	-44	45	0	8*mm*	CEN
RaPFC	44	45	0	8*mm*	CEN
LsPar	-50	-51	45	8*mm*	CEN
RsPar	50	-51	45	8*mm*	CEN
dACC	0	21	36	6*mm*	SN
LaPFC_SN	-35	45	30	8*mm*	SN
RaPFC_SN	32	45	30	8*mm*	SN
LIns	-41	3	6	6*mm*	SN
RIns	41	3	6	6*mm*	SN
LlPar_SN	-62	-45	30	8*mm*	SN
RlPar_SN	62	-45	30	8*mm*	SN

As seen in Table 1.1, nine nodes represent the Default Mode network, five represent the Control Executive network, and seven represent the Salience network. To be explicit, the lateral parietal cortices of the default mode network (LlPar & RlPar) refer to the bilateral angular gyri, and the lateral parietal cortices of the SN refer to the bilateral supramarginal gyri. The anterior prefrontal cortices of the CEN (LaPFC & RaPFC) refer to the inferior prefrontal gyri i.e., Brodmann area 45, and the anterior prefrontal gyri of the salience network refer to the superior frontal gyri. The reason 21 nodes were chosen is that very few studies with a large number of subjects used a large number of fully connected nodes. The most recent study that addresses the same topic, namely Zarghami et al., 2023 [86], utilizes more nodes and total connections, but does not create a fine-grained model that utilizes each node-node connection from multiple intrinsic brain networks. Therefore, using a relatively large number of nodes in a fully connected fashion with a relatively large sample size should provide useful and novel information about the differences in effective connectivity between the controls and patients within and between these three major brain networks. More nodes were not included due to the computational costs associated with estimating the dynamic causal models for each subject as the cost increases exponentially with each added node. The inclusion of multiple regions, including frontal, temporal, parietal, insular, thalamic, and cerebellar nuclei should give the basis for making meaningful insights into the differences in general neurophysiological activity patterns between the groups. How this is done will be described in detail in the methods. Before doing so, the research questions and hypotheses of this study are made explicit.

1.3. Research Questions and Hypotheses

The primary research questions of this thesis are:

1. Are there differences in effective connectivity between the control and patient groups? If so, where do they exist and where are they most prominent?

2. Are there differences in regional average Fractional Anisotropy (FA) values i.e., White Matter (WM) densities between the groups? If so, how do the differences found in this sample compare to existing findings related to this question?

3. From the EC metrics derived in the dynamic causal modeling process and calculations of average regional FAs, can a relationship between effective connectivity, fractional anisotropy, and disease severity be found that might implicate the role specific ROIs play in the severity of schizophrenia or impairment of cognition?

Answering these questions by using the data from this sample of relatively young people may give researchers and clinicians more insight into how schizophrenia spectrum disorders manifest, and how the complicated, varying symptoms associated with them might be driven by specific neurophysiological activities in the major brain networks used in this study. The hypotheses related to the questions are that:

1. There are differences in effective connectivity profiles between the groups, and the schizophrenic group should exhibit relatively high levels of inter-nodal and inter-network dysconnectivity.

2. The schizophrenic group will exhibit decreased WM density compared to the healthy controls in distributed areas of the brain; and

3. There will be an association between the effective connectivity metrics and the cognitive and clinical scores of the subjects, and an association between EC and FA metrics will be apparent as well.

2. Methods

In this chapter, the methods used to preprocess the raw multimodal MRI data, estimate and optimize Effective Connectivity (EC) metrics, calculate regional average Fractional Anisotropy (FA) metrics, and create composite cognitive scores of interest will be addressed. Additionally, the methods used to conduct the analyses of the relationships between the different modalities of data will be described in the two final sections of this chapter before the summary of the methods.

2.1. Preprocessing of resting state BOLD fMRI data

2.1.1. HCP minimal preprocessing of BOLD fMRI data

This HCP-EP data set was used in multiple studies in the Wohlschläger lab. I am using the description another Master's student, Ângelo Bumanglag, wrote on the BOLD fMRI preprocessing steps, that he used to prepare the data that were ultimately sent to me [11]. These quotes from his master's thesis are used with his permission. "The Minimal Preprocessing Pipeline for HCP data was utilized to process the data. The pre-processed structural data for 169 out of 183 subjects were readily available. This structural processing included removing readout distortion in the T1w and T2w images, aligning the images, correcting for bias field and registering them to standard spaces. The fMRI data was then subjected to the HCP functional pipeline, which implements steps from FMRIB Software Library (FSL) [43] and FreeSurfer [18] to account for distortions arising from choices such as multi-band acceleration, and higher spatial and temporal resolution. Specifically, the pipeline realigned the volumes to compensate for subject motion, registered the fMRI data to the structural images, reduced the bias field and normalized the 4D image to a global mean. To address distortion in the phase encoding direction, a pair of spin echo EPI scans were used with opposite phase encoding directions, which reversed the effect of B0 field inhomogeneity on the images. The minimal preprocessing pipelines aimed to minimize the loss of information during processing. Additional preprocessing such as spatial smoothing, temporal filtering, nuisance regression, or motion censoring (scrubbing) could result in significant loss of information [30]" [11]. In addition to the minimal preprocessing the data underwent before being shared with the lab, some corrections to systemic low frequency oscillations and quality control checks were performed; in this case these steps were also taken by Ângelo Bumanglag, and as such I will refer to his descriptions of the processes.

2.1.2. Rapidtide low-frequency oscillation correction

"The rapidtide[1] software package was used to estimate and remove systemic low frequency noise from resting state fMRI data. A time delay range of -10 to +10 seconds was used, and to determine the time delay in each voxel, rapidtide yields the maximum cross-correlation between the BOLD signal in a given voxel and a reference time course, that is obtained from the whole brain signal. Additionally, the data are temporally bandpass filtered between 0.01 and 0.15Hz, which is typically where the signal fluctuations of interest reside in rs-fMRI data [76]. Finally, a General Linear Model (GLM) filter is used to remove the physiological signal, leaving only the "pure" neuronal signal for further analysis" [11]. This section was transcribed nearly verbatim to what was written in Ângelo Bumanglag's thesis report. The following section on Quality Control is the final section in which this will be the case.

2.1.3. Quality Control

"Functional preprocessing was conducted on 169 subjects. However, 5 subjects were excluded from the analysis due to voxel merging inconsistency and failure to estimate the distortion field. Head motion is a significant source of noise in fMRI signals, and it can introduce systematic bias in case-control studies if not appropriately controlled [55]. To estimate head motion during the fMRI scan, the MCFLIRT algorithm from FSL was employed. This algorithm summarizes the translational and rotational movement of the head along the X, Y , Z, ϕ, θ, and ψ axes [44]. Strict exclusion criteria were implemented, and subjects were excluded if they met at least one of the following: multiple consecutive volumes displaced by more than 3mm or 5°. This resulted in the exclusion of 6 scans with AP phase encoding direction and 4 scans with the PA direction. Therefore, the final data-set was comprised of 156 subjects with scans in the AP encoding direction and 158 subjects with scans in the PA direction. [11]." After these processes were complete, the data were sent to me for further processing and analysis within the scope of this thesis. Those further processing steps, model estimations, and analyses are described throughout the remainder of the methods.

2.1.4. Further processing of the resting state BOLD fMRI data

After minimal preprocessing via the HCP functional pipeline, corrections for systemic low frequency oscillations via the rapidtide software package, and quality control for excessive head movement or other inconsistencies, the data were subjected to further processing to prepare them for spectral dynamic causal model estimation. First, the data were smoothed using a $6mm$ Full width half maximum (FWHM) kernal. These smoothed images were subsequently bandpass filtered into slow 5 (0.01 to 0.027Hz) and slow 4 (0.027 to 0.073Hz) frequency bands using DPABI's **y_bandpass** function, that implements an ideal rectangular filter to do so [83]. The filtered data were passed to two separate General Linear Models (GLMs) using Statistical Parametric Mapping (SPM) version 12[2]. The design matrices contained a discrete cosine

[1] `https://github.com/bbfrederick/rapidtide`

[2] `https://www.fil.ion.ucl.ac.uk/spm/software/spm12/`

basis set spanning either the slow 5 or slow 4 frequency bands. Subject head motion and Cerebro-Spinal Fluid (CSF) signal from the 4*th* ventricle were included in the design matrix as nuisance regressors to the models. This resulted in two F-contrasts being specified over the DCT basis sets. The maximum F-contrast value in each spherical ROI was identified, and a new sphere was centered at the location of that maximum value; See Table 1.1 for the positions and diameters of the nodes that defined the boundaries of the searches. Notably, a brain mask was used in concurrence with this process, and if a sphere's centroid ended up on the edge of the brain, non-brain regions were not accounted for in the stored average time series. Similarly, in edge cases where voxels in the brain mask had a positive value but the time series contained an undefined value, the information from that voxel would not be included in the average time series calcuation. The average signal intensity from each of the re-centered spheres was calculated for each time point in both frequency bands using SPM12's VOI utility function, which resulted in storing two average time courses for each ROI for each subject. These time series were then passed to a sp-DCM estimation procedure, that was implemented using the **spm_dcm_fmri_csd.m** function from SPM12. The method implemented via that function is described in the following section.

2.2. Spectral Dynamic Causal Model estimation

This section provides a brief description about what spectral dynamic causal models are and how they have been used in this project. More complete details about this family of models, their origins, and how they compare to other directed effect models can be found in a series of publications by the developers of the method [26] [61] [27] [60] and other researchers who have utilized it. See the following works for examples of its use in the case of examining endogenous dynamics in the schizophrenic brain [86] [89] [14].

Generally speaking for the case of BOLD fMRI data, the spectral dynamic causal model estimation algorithms deployed in SPM12 take haemodynamic time series data and use a Fourier transform to obtain information about the observed complex cross spectra of the data recorded from each node. This information is passed to a generative model that estimates an intrinsic connectivity matrix 'A' by using an iterative variational Laplace algorithm to obtain maximum likelihood state space parameter values, that control the amplitudes and exponents of the observed spectral densities and observation error. A more precise description is provided in the original publication that the method appears in, which is Friston et al., 2014 [26]; the construct validity of the model is addressed in Razi et al., 2015 [60], and I have also found the description used in section 2.5.1 of the work of Zarghami et al., 2023 to be succinct and representative of the methods used here [86]. It should also be noted that functional connectivity priors were used to induce parameter constraints in the model estimation as described in Razi et al., 2017 [61] and Seghier and Friston, 2013 [64].

After implementing this method, we are left with a maximum likelihood posterior expectations of the endogenous effective connectivity between each node. As such, we have estimated a fully connected (21 by 21) 'A' matrix in two frequency bands for 96 subjects, ultimately resulting in 96 x 2 individual endogenous connectivity matrices with 441 elements each.

These models were estimated by using the **spm_dcm_fmri_csd.m** script from SPM12, and was called using a 'True' value for the two-state option meaning that the generative model took into account a hidden state for both excitatory and inhibitory populations of neurons for each node. All other options took default values. The maximum number of iterations for the estimation of each model was the default value of 128, and the time series was scaled by a default precision value of 4. If a subject's model failed to converge before reaching the 128th iteration or if SPM threw a singularity warning stating that the model may be badly scaled or inaccurate, then the subject was excluded from the ensuing analyses.

2.2.1. Exclusion of Subjects based on DCM estimations

38 subjects were excluded due to singularity warnings thrown during the estimation of the first level sp-DCM either in the slow 5 or slow 4 model. 3 subjects were excluded because either their slow 5 or slow 4 model did not converge after 128 iterations. An additional 19 subjects were excluded due to being in the 'affective psychosis' group, who are not the primary focus of this study. Finally, two subjects were removed due to having at least one maximum F-contrast value outside of the search radii of the ROIs of interest. This leaves us with the 96 subjects that are used throughout the remainder of the study, 57 of whom are patients and 39 of whom are controls. 45 of those patients have complete cognitive score information, and 31 of the controls have complete cognitive score information.

2.3. Parametric Empirical Bayes

Once a spectral dynamic causal model was estimated for each frequency band for each subject, the models were subjected to optimization with Parametric Empirical Bayes (PEB) [23] [24] [19] implemented via **spm_dcm_peb.m**. A design matrix was supplied to this algorithm that contained a column consisting of only ones and a binary covariate specifying whether each subject belonged to the healthy control group or the non-affective psychosis (schizophrenic) group. This results in both the estimation of the average effective connectivity for each node to node connection for the control group, and the difference in average connectivity strength for each connection between the groups. This method has been used in several studies investigating EC in schizophrenia, e.g., Zarghami et al., 2023 [86], Zhou et al., 2018 [89], and Csukly et al., 2019 [14].

2.4. Bayesian Model Reduction

The EC estimates of the PEB models were further optimized via Bayesian Model Reduction (BMR) [22] [24] implemented via **spm_dcm_bmr.m** in SPM12. This process essentially optimizes the posterior expectations and corresponding variances of the effective connectivity values by evaluating model information in an iterative procedure that leaves relatively uninformative connections of the fully connected model out until the next connections that would be pruned are identified as contributing to model information; then, once the best

256 models were identified, a weighted average of the estimated parameters was calculated using Bayesian Parameter Averaging. Zhou et al., 2018 also describes this process in a more complete fashion in section 2.7.4 of their publication [89]. The information of a given reduced PEB model is quantified by that model's free energy. For more details on this definition and on the BMR process see Friston et al., 2007 [20] and Friston, Parr, and Zeidman, 2018 [22]. The reduced models yield the final metrics that will be used in this study for the analyses of differences in EC profiles between groups and the correlations of EC values to cognitive and clinical scores.

2.4.1. Assessing differences in EC

To evaluate whether any given connection strength statistically significantly differed between the groups, the posterior estimates of expected differences in effective connectivity between groups from these reduced models were compared to the posterior estimates of the corresponding variances. If the absolute value of the estimate of the difference in EC was greater than two times the associated standard deviation, then that difference was considered to be statistically significant. Corrections for multiple comparisons were not made as the works of Zeidman et al., 2019, Gelman et al., 2012, Gelman and Tuerlinckx, 2000, and Neath et al., 2018 were cited in the work of Zarghami et al., 2023 to make the statement that "...the hierarchical nature of PEB along with precise null priors specified for the group effects [87] automatically (and stringently) adjusts for multiple comparisons [28] [29] [53]" [86].

The EC values derived from this work are visualized in a series of square plots in the results section, where all group-wise posterior expectations and the posterior expectations of differences between the groups are plotted (See: Figure 3.1), and the statistically significant differences are represented in Figure 3.2. The statistically significant differences in EC are also visualized in a series of four circular connectivity plots in the following subsection; See Figure 3.4 through Figure 3.7.

To assess the qualitative differences in EC values between the groups, a metric was derived to indicate whether a connection that was either non-existent, excitatory, or inhibitory in the control group possessed a different quality in the schizophrenic group. If for example a strongly excitatory connection was present in the control group between two given nodes and that same connection in the schizophrenic group was non-existent or inhibitory, then the metric would be negative and scaled by the absolute difference in connectivity strength. Positive values reflect that either the connection for the control group is non-existent or inhibitory and that for the schizophrenic group the connection is excitatory (or non-existent in the schizophrenic group if the control group's connectivity strength for that node is inhibitory). A connection strength was considered to be 'non-existent', or in other words neither inhibitory or excitatory, if the associated EC value was within the range of -0.0001 and 0.0001 Hz. These differences are displayed in Figure 3.3, and are described in the corresponding section of the results.

Inspired again by the work of Razi et al., 2017 [61], the source-sink profiles of each node were calculated in each frequency band. This metric quantifies the weighted strength of connections entering and exiting the node. In this case, a source-sink profile was calculated

for both excitatory and inhibitory connection types in isolation. These results are displayed in a series of scatter plots: See Figure 3.8 through Figure 3.11. Diagonal elements of the 'A' matrix were excluded from this part of the analysis as they are scaled to reflect self-inhibitory connectivity rather than actual EC, which the off-diagonal elements represent.

2.5. Raw Diffusion Weighted Image data preprocessing

Raw Diffusion Magnetic Resonance Imaging (dMRI) data were preprocessed using a pipeline that I developed in a previous project[3], that is similar in nature to the official HCP minimal preprocessing pipeline for dMRI[4]. In the pipeline I developed, the data were first denoised using MRTrix3's **dwidenoise** function, that employs Marcenko-Pastur Principal Component Analysis (PCA) denoising to target Gaussian noise in the signal [77] [79] [80] [13]. These denoised data were passed to the MRtrix3 function **mrdegibbs**, that corrected the images for Gibbs ringing artefacts [77] [46] [8].

The following steps rely on the FMRIB Software Library (FSL) toolbox [43]. After the Gibbs ringing correction, the non-diffusion weighted volumes from the data collected in both encoding directions were evaluated, and the volumes most closely resembling the average of all the non-diffusion weighted images were isolated. These two 'most average' volumes were then merged into a 4-D non-diffusion weighted image where the first 3-D volume was the most average non-diffusion weighted image acquired in the Anterior-Posterior (AP) encoding direction, and the second was the most average from the reverse encoding direction (PA). These images were then used as an input to FSL's **topup** algorithm. The algorithm is described in the FSL documentation as behaving to use these pairs of reverse phase-encoded volumes to "estimate the susceptibility-induced off-resonance field using a similar method to that described in Andersson et al., 2003, [2] as implemented in FSL [70] and the two images were combined into a single corected one"; and that "for a comparison of the performance of **topup** compared to "traditional" dual echo-time gradient echo fieldmaps [the reader] may also be interested in Graham and other's 2017 publication [31]". These corrections were applied to the images using FSL's **applytopup** function.

After these correction steps, the presence of eddy currents in the images was addressed using FSL's related tools. As the correction for eddy currents is described by them, for each subject "the susceptibility induced off-resonance field was estimated from spin-echo EPI images acquired with different phase-encoding directions [2] [as described above]. This field was passed to "**eddy**", a tool that combined it with estimating gross subject movement and eddy current-induced distortions [3]. The quality of the dataset was assessed using the eddy QC tools [7]. Slices with signal loss caused by subject movement coinciding with the diffusion encoding were detected and replaced by predictions made by a Gaussian Process [1]." From there, **fslmaths** was used to calculate the mean of all the non-diffusion weighted volumes from the full 4D eddy corrected image. The eddy corrected data and average non-diffusion

[3] `https://github.com/CJones770/tractography-pipeline-restore`

[4] `https://github.com/Washington-University/HCPpipelines/wiki/Installation-and-Usage-Instructions#diffusion-preprocessing`

weighted images were then smoothed using a $1mm^3$ Gaussian kernel. These images were used as inputs for the estimation of Diffusion Tensors via FSL's Bayesian Estimation of Diffusion Parameters using Sampling Techniques (BEDPOSTX) [9] [40] on a Graphics Processing Unit (GPU) [36], where the X refers to modeling crossing fibers [41]. Notably, the rician noise modeling flag was turned on in this step of the processing. These processes ultimately provide estimates of Fractional Anisotropy and Mean Diffusivity in three principal diffusion directions for each subject, of which the former will be used to assess differences in regional average fractional anisotropies between the groups. More details about the BEDPOSTX workflow is available at the FSL wiki[5]

After the FA values were estimated, the subject space images were normalized to the $2mm$ MNI-152 standard space with the **FLIRT** command from the FSL [43] toolbox in order to conduct group difference analyses across various ROIs in $2mm$ atlas spaces of interest.

2.6. Choosing standard spaces for FA analyses

In order to test for differences in regional average Fractional Anisotropy (FA), and subsequently make inferences about differences in White Matter (WM) density between the groups, Regions of Interest (ROIs) in the diffusion weighted image space must be specified. To do this, here supplementary images from the 2018 work of O'muircheartaigh and Jbabdi [54] were used as they created and published a set of white matter tracts that stemmed from a set of grey matter independent components. This may give a data-driven basis for assessing how distributed white matter tracts connected to major grey matter nuclei may differ between the groups. The specific files that were used from their supplementary materials are called 'SI-7-ICsCortex050_MM.dtseries.nii', which contains the grey matter parcels, and 'SI-9-ICsTracts050_MM_2mm.nii.gz'. which contains the white matter tract volumes. Notably, the tracts published in the O'muircheartaigh and Jbabdi work were not generated using any patient populations. Therefore, the applicability to this case may be limited, nevertheless, given that the concurrent white and grey matter populations are not typically accounted for in atlases covering distributed regions of the brain, they will be used anyway and subsequently corroborated by a more traditional approach of using a white matter atlas. In this case, the white matter components of the Talairach atlas [74] made available in the FSL [47] [48] toolbox will be used.

2.6.1. O'muircheartaigh and Jbabdi Independent Components

This section briefly summarizes the processes O'muircheartaigh and Jbabdi used to create the concurrent grey and white matter ICs in their 2018 publication [54]. Initially, they conducted a whole-brain tractography over 37 subjects using FSL's **probtrackx2**[6] functionality using a set of "9127 subcortical voxels...and...59,412 cortical vertices (seeded from the mid grey matter surface, excluding the non-cortical medial wall)..."as seed regions [54]. The probabilistic

[5] `https://fsl.fmrib.ox.ac.uk/fsl/fslwiki/FDT/UserGuide`

[6] `https://fsl.fmrib.ox.ac.uk/fsl/fslwiki/FDT/UserGuide#ProbtrackX_outputs`

tractography outputs of this process, which represent white matter tract density, were then averaged and passed to "an adapted incremental method referred to as Melodic's Incremental Groupwise Principal Component Analysis (PCA) (MIGP) in Smith et al., 2014 [71]" [54]. The dimensionality of the outputs of these processes were further reduced via the "**fastICA** algorithm" [54]. The volumes from their supplementary materials that are used in this paper as a standard space for assessing differences in regional average fractional anisotropy are from the ICA that reduced the dimensionality of the concurrent white and grey matter bundles to 50 sets of volumes; i.e., "SI-7-ICsCortex050_MM.dtseries,nii", which contains the grey matter volumes, and "SI-9-ICsTracts050_2mm.nii.gz", which contains the white matter tracts [54].

The full description of the methods I summarized can be found in their original publication under the subsections "Diffusion data preprocessing and tractogrpahy" and "Independent component analysis of tractography data" [54]. This is not a perfect set of volumes to use as a standard space, as even the authors admit that a constraint of their methods is that the resulting volumes are "a sample-specific template" and that "...probabilistic tractography does not directly quantify white matter integrity, but rather our uncertainty on streamlines through the diffusion field [42]" [54]. However, it still may prove interesting to evaluate whether fractional anisotropy within these estimated white matter tracts, that are evidently connected to specific grey matter volumes differ between the control and schizophrenic groups.

2.6.2. Talairach atlas White Matter Regions

To reconcile the shortcomings mentioned in the previous subsection, a more established standard space is used in concurrence with the volumes produced by O'muircheartaigh and Jbabdi [54], namely, the Talairach atlas. This atlas was first developed in 1988 by Talairach et al. [74] and includes neuroanatomical structures that are "orgainzed into five hierarchical levels: hemisphere, lobe, gyrus, tissue type, and cell type" as shown in Figure 1 of Lancaster et al., 2000 [47]. The Lancaster et al., 2000 publication describes the process by which this atlas was digitized and labeled [47]. More details about the atlas are available on the FSL wiki[7]. For a description of how the use of multiple atlases can result in the emergence of spatial bias in imaging data, the reader is directed to Lancaster et al., 2007 [48]. In this study, the regions with white matter tissue type identifiers that consisted of at least 10 voxels are isolated and used to define a set of standard ROIs across which differences in average fractional anisotropy between the control and schizophrenic groups can be tested.

2.7. Calculating regional average fractional anisotropies

Now that the regions have been defined, the method by which regional average fractional anisotropies are calculated will be described. In the case of the O'muircheartaigh and Jbabdi ICs, both non-weighted and weighted average FAs were calculated. The non-weighted average regional FAs were calculated simply by taking the sum of the FA values from voxels within the given ROI that were identified as being white matter by a tissue segmentation process

[7] `https://fsl.fmrib.ox.ac.uk/fsl/fslwiki/Atlases`

implemented via SPM, and subsequently dividing that sum by the number of included voxels. This results in a simple estimate of average regional FA over the 50 ICs provided by O'muircheartaigh and Jbabdi [54]. For the weighted averages, each voxel's FA value was multiplied by the weight associated with it in the O'muircheartaigh and Jbabdi probabilistic white matter tracts, thereby relatively increasing the contribution of voxels that are most connected to the seed region in the calculation of the average. Given that the Talairach atlas is not probabilistic, no such weighting was conducted and the results that are shown in the following chapter are reflective of that. Differences in mean regional average FA were conducted via one-sided t-tests with the alternative hypothesis being that average regional FA would be reduced on average in the schizophrenic group for each region. Each p-value was corrected for multiple comparisons using false discovery rate (FDR) correction within each individual family of tests across ROIs; i.e., p-values from the non-weighted O'muircheartaigh and Jbabdi ICs were corrected independently from the other groups, and the same is true for the weighted FA values and the Talairach based averages. FDR correction was implemented using the Benjamini-Hochberg method [10] as implemented via the **fdrcorrection** function in the statsmodels.stats.multitest Python package.

2.8. Regressing groups on cognitive scores

To test for differences in cognitive scores between the groups while controlling for the sex of the subjects and the occasional interaction term as found appropriate, simple multiple regression analyses were conducted for the cognitive variables of interest. The only covariate that was controlled for in this case was sex due to the fact that there is a significant difference in the average age of the subjects between the groups, therefore introducing age as an independent variable to the analysis would induce substantial multicollinearity to the model, potentially interfering with the estimates of group differences. While this statistically significantly different age profile of the groups is grounds for concerns, we may find some relief in the relatively minor practical difference between the average ages of the groups, where both groups have an average age in the low to mid 20s; See Figure 1.1 for demographic information about the groups.

2.9. Comparing Effective Connectivity to Cognitive Scores with Canonical Variate Analysis (CVA)

Canonical Variate Analysis (CVA), also known as canonical correlation analysis, is one of the methods prescribed in the work of Friston et al., 2016 [24] for evaluating the relationship between effective connectivity features and behavioral metrics. The **spm_cva** function was used to generate the models, and as per the documentation in the script "CVA uses the generalised eigenvalue solution to the treatment and residual sum of squares and products of a general linear model. The eigenvalues (i.e., canonical values), after transformation, have a chi-squared distribution and allow one to test the null hypothesis that the mapping is D or

more dimensional."; In this thesis, only the results for the test of D being equal to one are presented, and as such "the first p-value is formally identical to that obtained using Wilks' lambda and tests for the significance of any mapping."; the **spm_cva** function was written by Karl Friston and is available in the SPM version 12 software package. The CVA method has been used in other studies evaluating the relationship between endogenous connectivity features derived from dynamic causal modeling of resting state fMRI data and clinical or cognitive scores; this method was notably used in a contemporary study by Zarghami et al., published in 2023 [86] and in another recent study by Zhou et al., 2018 [89]. This paper will attempt to emulate the methods used in the work of Zharghami et al., as they raise important points about over-fitting and over-sensitivity issues of the CVA method when utilizing too many features compared to the number of subjects included in the model. They reference that "based on previous rigorous studies [of] (Helmer et al., 2020 [35]; Leach & Henson, 2014 [49]; Yang et al., 2021 [84]), constructing reliable CCA models requires that the number of samples be at least 9-10 times the number of features" [86]. Their study has an original feature to subject ratio similar to this study, where they had "58 schizophrenic subjects with cognitive score data available and 470 EC features" [86], and this study has 45 schizophrenic subjects with all cognitive scores available and 441 EC features. Therefore, it seems fitting to use the same feature selection methods employed in their work to better meet the criteria for constructing a reliable CVA model.

2.9.1. Feature Selection for CVA

In Zarghami et al., 2023, the feature selection process is described in section 2.6.2 [86]. In it is the description of the selection process of the most relevant EC features and cognitive scores that are passed to a final CVA model. Those CVA models ultimately aim to describe how the EC values of given node to node connections relate to the observed variance in the selected cognitive and clinical scores within the schizophrenic group. To select these features "[a] forward selection on the EC parameters followed by backward elimination on the [cognitive] scores [was used]..." [86]. The technical details are available in their publication; to paraphrase the processes they describe, in the forward selection process a CVA model is created across all of the cognitive scores using one EC feature at a time, and the most descriptive features (or connections) are stored until a fixed number of best descriptive features is reached. These features are then used in a subsequent series of CVA models that first utilize all of the relevant and available cognitive scores, then cognitive scores are removed one by one, removing the least significant, or most redundant, cognitive scores until the next cognitive score that would be removed was statistically significant [86]. The same process was used for the clinical (PANSS) scores in this study. Given that there are two model families (one per frequency band) and two dependent variable families of interest (cognitive and clinical scores), this study has generated four CVA models. It should be noted that unlike the methods in the Zarghami et al., 2023 publication [86], this study did not implement the "bootstrap aggregating (aka bagging)" technique to select features, therefore our models may not be as "resistant to small changes in the data"; additionally, the generalizability of our models were not assessed via "k-fold cross-validation" as was done in the Zarghami et al.,

2023 publication (section 2.6.3) [86]; it is intended that these differences in methods will be addressed in preparing this thesis for publication in the near future.

In order to limit the number of features that would be chosen in the feature selection process for this study while retaining their information, the cognitive scores were condensed into composite scores. The cognitive scores that were passed to the selection process were: The area under the curve metric for the delayed discounting task ($40,000), the total number of correct responses in the emotion recognition task divided by the log reaction time for correct responses, and the average of each subject's fluid and crystallized cognition scores. The clinical scores, which are the four PANSS subscores, were entered into the feature selection unaltered.

2.10. Summary of the methods

In summary, each of the methods used to generate results in this study are as follows: First, a fully connected Spectral Dynamic Causal Model (sp-DCM) was generated for each subject using information from the slow 5 frequency band in one case and the slow 4 band in the other. Second, those models were reduced using Parametric Empirical Bayes (PEB), and the estimates from those models were optimized using Bayesian Model Reduction (BMR). At this point the EC values for each connection and the differences between the groups were estimated, and the results are presented in Figure 3.1, Figure 3.2, and Figure 3.3; The figures display the average EC values in each group, the statistically significant differences between the groups, and the qualitative differences in connectivity between the groups, respectively.

Then, regional average Fractional Anisotropy (FA) values were calculated over two 'standard spaces', namely a set of ICs from the work of O'muircheartaigh and Jbabdi, 2018 [54] and the white matter regions of the Talairach atlas [47] [48]. The regional average FA values calculated within the ROIs were compared between the control and schizophrenic groups using a set of one-sided t-tests with an alternative hypothesis that on average the schizophrenic group would exhibit reduced regional average FA. The p-values resulting from these tests were subsequently corrected for multiple testing using false discovery rate (FDR) correction with the Benjamini-Hochberg method [10].

Then, group differences in cognitive scores were evaluated via linear regression using the group variable (i.e., whether the subject was in the control or patient group), and sex as a covariate for each cognitive score. The cognitive scores that were used were: A composite score of auditory hit rates and response times in the Seidmann auditory continous performance test (acpt), delayed discounting tasks to evaluate the present value of $40,000 at 6 months and 10 years into the future, composite scores of fluid and crystallized cognition, and the number of correct responses and reaction time for those correct responses in the Penn emotion recognition tasks. The regression tables for these analyses are found in the general addenda (See Figure A.1 - Figure A.10).

Finally, the effective connectivity scores were correlated to the cognitive scores using Canonical Variate Analysis (CVA). The processes used are described in the previous two subsections of this chapter. The results are described in Figure 3.13 through Figure 3.24.

3. Statistical Analyses and Results

In this section, the results generated from the processes described in the previous chapter and the analytical methods used to evaluate them are presented and briefly commented on. Further interpretations of the results with respect to existing findings in the literature will be made in the following discussion chapter.

3.1. Differences in Effective Connectivity

3.1.1. Reduced PEB models (Bayesian Model Reduction (BMR))

The group average EC of each connection in each frequency band and the differences in EC values between the groups are visualized in Figure 3.1. The directed effect is read as being from column X to row Y. The EC values representing differences between the groups with magnitudes greater than two times their respective standard deviations were interpreted as being statistically significant, and are presented in the second set of carpet plots in this section (See Figure 3.2). Numeric information about the top 10% of differences in EC values between the groups and whether they are statistically significant or not can be found in the supplementary materials; these top 10% contain all statistically significant differences in EC strength between the groups. From the square plots it can be seen that in the slow 5 frequency band the schizophrenic group exhibits relatively increased inhibition in 25 of the 441 connections with only four connections exhibiting increased excitation, and that in the slow 4 frequency band there is a mix of increased inhibition and excitation across the modeled connections; 12 connections are relatively more inhibitory in the slow 4 band in the schizophrenic group, and 14 connections are relatively more excitatory. These connections are also visualized in circular plots in section 3.2.

Differences in EC between the groups that are reflective of qualitative differences in the connection are shown in Figure 3.3. It is clear from the plot that in the slow 5 frequency band, the schizophrenic group exhibits connectivity qualities that are different and relatively more inhibitory than those observed in the control group. Negative metrics in this plot reflect the case where the control group exhibits a non-existent connection and the schizophrenic group exhibits an inhibitory connection, or where the control group exhibits an excitatory connection and the patient group exhibits either a non-existent or inhibitory connection. The same style of logic is applied in reverse for the positive metrics shown in Figure 3.3. It should be noted that these qualitative differences do not convey any information about statistical significance, whereas the differences identified in the previous paragraph and in Figure 3.2 do.

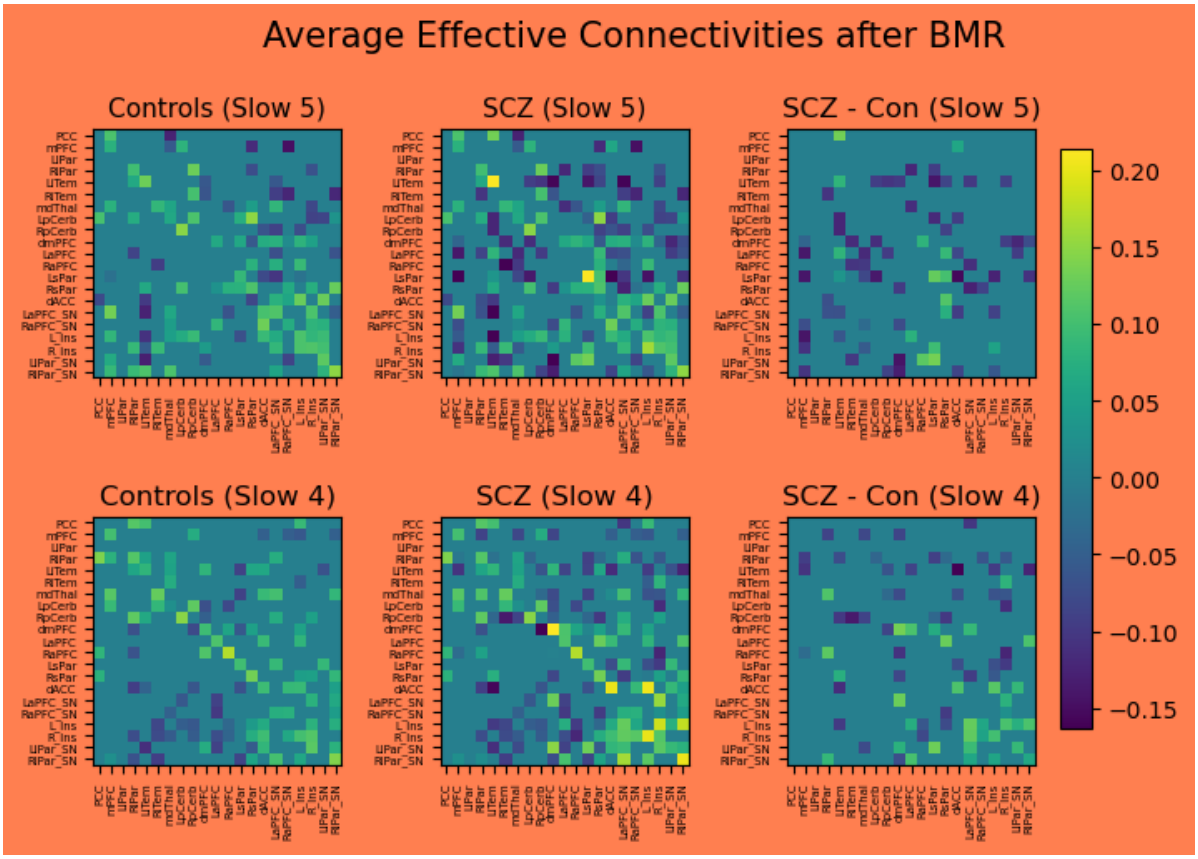

Figure 3.1.: Posterior expectations of group average effective connectivity and the differences between the groups after BMR

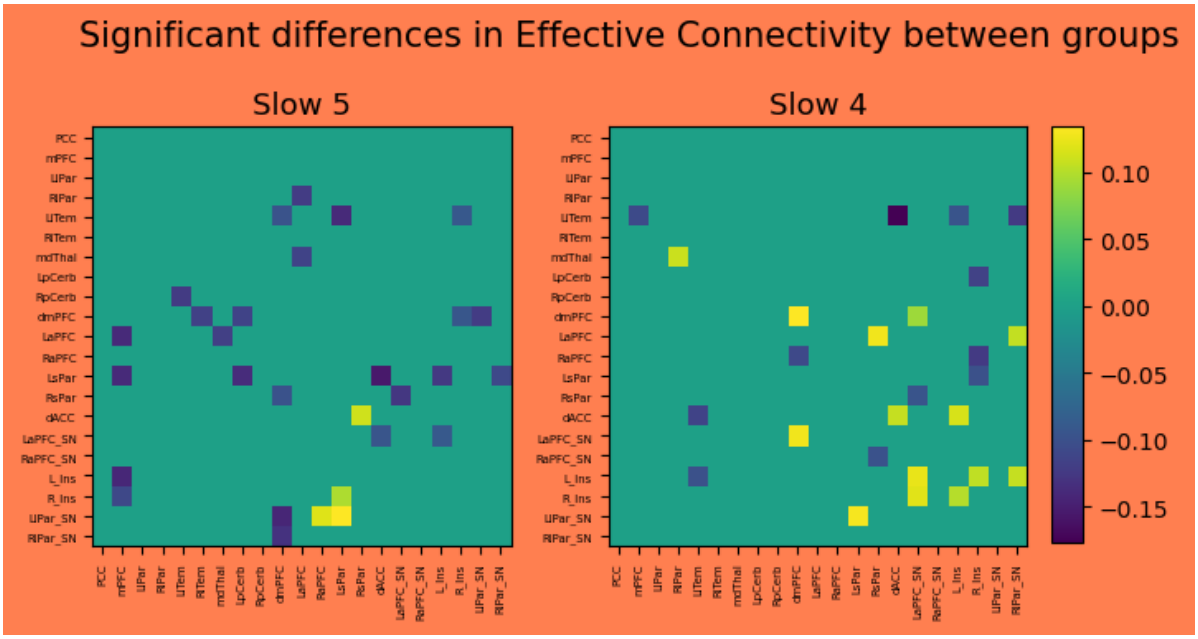

Figure 3.2.: Statistically significant differences in effective connectivity estimates post BMR.

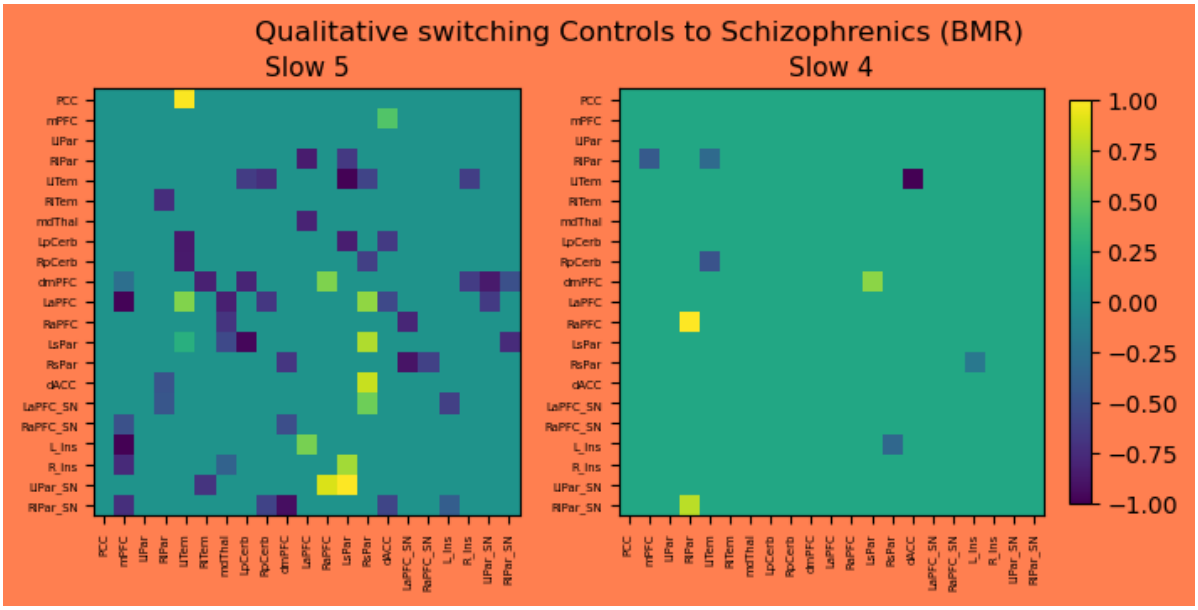

Figure 3.3.: Square plots indicating the direction and magnitude of differences in effective connectivty estimated from the reduced second level models if the quality of the connection differed between the groups. E.g., if at a given node the control group had a positive value or zero value, and the schizophrenic group had a negative value (indicating an excitatory, non-existant, or inhibitory connection, respectively), then the plot would indicate a negative value scaled by the difference in the strength of the connection in each group.

3.1.2. Proportions of altered connections within and between networks

In the recent study of Zarghami et al., 2023, the authors commented on the proportion of altered connections within each network that they modeled [86]. This work will report the differences in EC estimates similarly, however, given that in this work between network connections were modeled the proportion of altered between network connections will be commented on as well. Each proportion is rounded to two decimal places.

Within the DMN, which contains 81 total connections, the proportion of altered connections between the groups was 1.23% in the slow 5 frequency band and 2.47% in the slow 4 band. Of the 45 connections projecting from the DMN to the CEN 6.67% were altered in the slow 5 band, and 0 were altered in the slow 4 band. Of the 63 connections projecting from the DMN to the SN 1.59% of connections were altered in the slow 5 band and 4.76% were altered in the slow 4 band. Of the 45 connections from the CEN to the DMN 8.89% were altered in the slow 5 band and 0% were altered in the slow 4 band. Of the 25 connections within the CEN, 0% were altered in the slow 5 band and 4% were altered in the slow 4 band. Of the 35 connections from the CEN to the SN 8.57% were altered in the slow 5 band and 11.43% were altered in the slow 4 band. Of the 63 connections from the SN to the DMN 3.17% were altered in the slow 5 band and 1.59% were altered in the slow 4 band. Of the 35 connections from the SN to the CEN 8.57% were altered in the slow 5 band and 5.71% were altered in the slow 4 band. Finally, of the 49 connections within the SN 2.04% were altered in the slow 5 band and 10.2% were altered in the slow 4 band. Out of the total 441 connections, 29 were significantly altered in the slow 5 band (6.58%) and 26 were altered in the slow 4 band (5.89%).

The intra and inter-network connections with the largest proportions of statistically significantly altered strengths in node to node effective connectivity are the CEN to the SN in the slow 4 band with 11.43% of the connections being altered and in the slow 5 band with 8.57% being altered. This is followed by the intra-SN connections in the slow 4 band, where 10.2% of the connections are significantly altered. In the slow 5 frequency band a relatively large proportion of connections projecting from the CEN to the DMN (8.89%) are altered, and in the connections from the DMN to the CEN 6.67% of connections were altered. These results suggest that the greatest proportion of differences in EC in the slow 4 frequency band between the control and schizophrenic groups is represented by altered EC in the connections from the CEN to the SN and in the intra-SN connections; and in the slow 5 band the greatest proportion of EC alterations exist in the reciprocal connections of the nodes of the CEN and DMN and in the connectivity from the CEN to the SN. These findings are further visualized in the ensuing section.

3.2. Circular Plots

The differences in effective connectivity between the groups can also be represented in circular plots, which more visually intuitively indicate differences in network-network integration. See: Figure 3.4, that shows the connections in the model that are statistically significantly more inhibitory in the schizophrenic group in the slow 4 frequency band; Figure 3.5, which shows the same but using the slow 5 frequency band models; Figure 3.6, shows differences

in connectivity in the slow 4 frequency band based models that are more excitatory in the schizophrenic group; and Figure 3.7, that shows the same but in the slow 5 frequency band based models. The differences that indicate relatively more excitatory connectivity in the schizophrenic group are denoted by green arrows, and those that are relatively more inhibitory are denoted by red arrows. The nodes of the default mode network are denoted by red lines between the node labels in the outer circle of the diagram; the nodes of the control executive network are marked by green separators, and the nodes of the salience network are marked by blue separators. The crescents in the space between the arrows and the label names represent the proportion of connections leaving the node, or out strength in orange, and the number of connections entering the node, or in strength in blue. The circular plots were generated using a modified version of matlab functions published in Sizemore and Basset, 2018 [69]. The link to the github page corresponding to their study is listed below[1].

[1] `https://github.com/asizemore/Dynamic-Graph-Metrics`

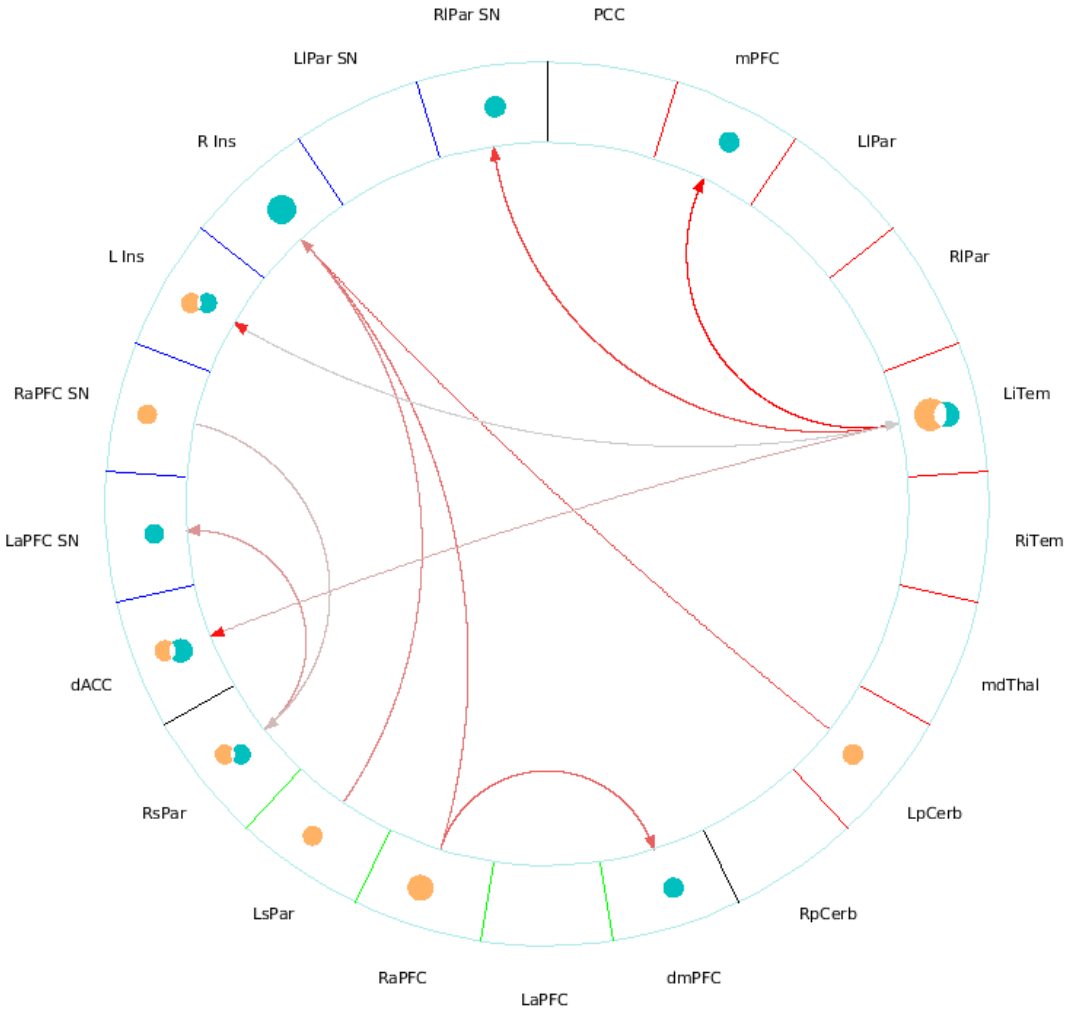

Figure 3.4.: Circular (Sizemore) plot representing significant differences in EC where connections are more inhibitory in the schizophrenic group compared to the controls in the slow 4 frequency band. The red region indicates the DMN, the green region indicates the CEN, and the blue region represents the SN.

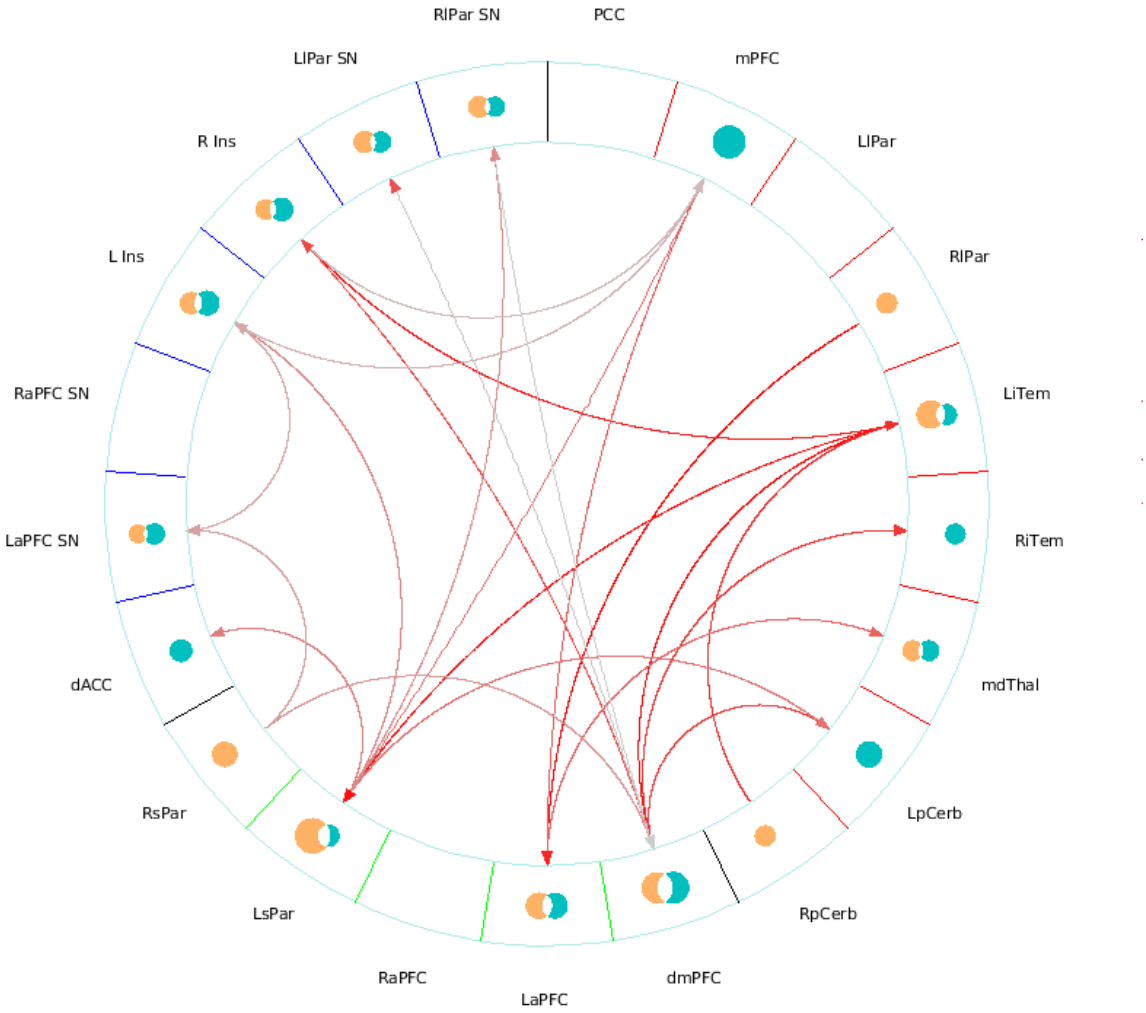

Figure 3.5.: Circular (Sizemore) plot representing the significant differences in EC where connections are more inhibitory in the schizophrenic group compared to the controls in the slow 5 frequency band. The red region indicates the DMN, the green region indicates the CEN, and the blue region represents the SN.

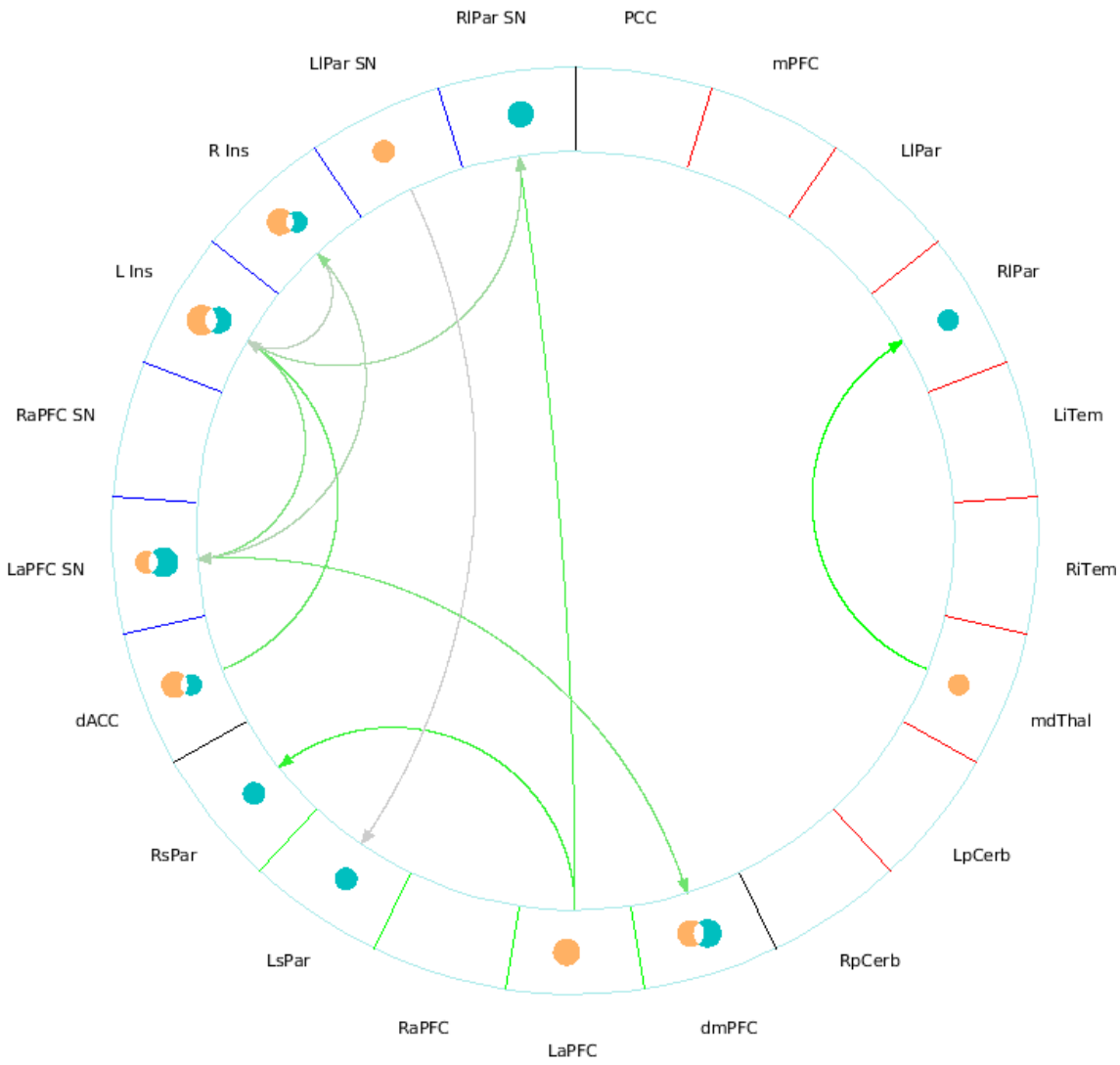

Figure 3.6.: Circular (Sizemore) plot representing the significant differences in EC where connections are more excitatory in the schizophrenic group compared to the controls in the slow 4 frequency band. The red region indicates the DMN, the green region indicates the CEN, and the blue region represents the SN.

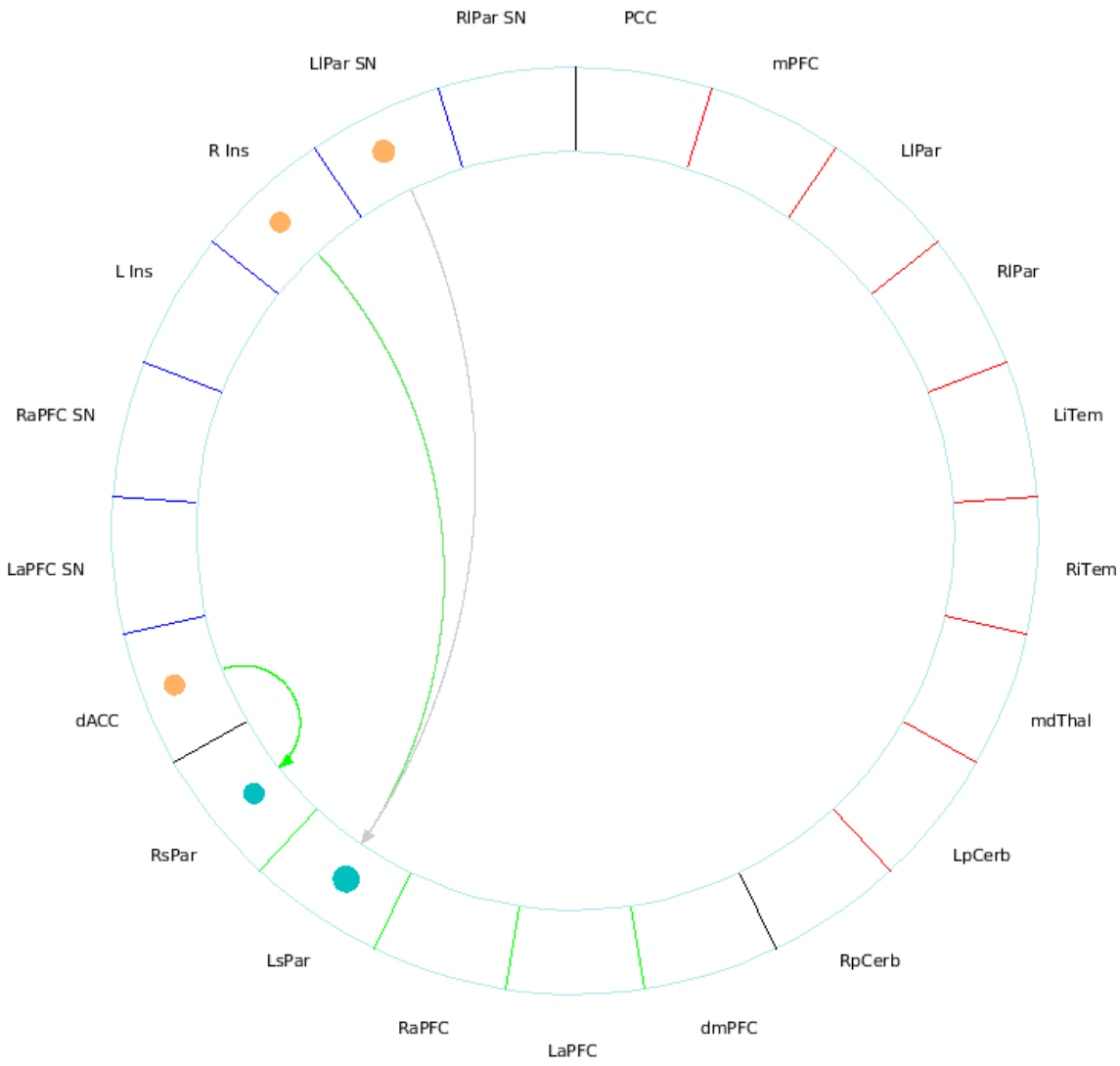

Figure 3.7.: Circular (Sizemore) plot representing the significant differences in EC where connections are more excitatory in the schizophrenic group compared to the controls in the slow 5 frequency band. The red region indicates the DMN, the green region indicates the CEN, and the blue region represents the SN.

3.3. Source-Sink profiles

A method that was employed in Razi et al., 2017 [61] was to calculate the weighted ratios of in-strength and out-strength for each node, ultimately quantifying the total number and strength of connections entering and leaving said node. By doing so, we gain information about whether there is asymmetry between nodes in the left or right hemispheres, which was the original purpose as described in their work; and additionally, in this case given that we are making comparisons between groups, we gain information about whether nodes in either group behave more like sources or sinks relative to the other group, and we quantify how strongly connected a given node is in either group. The following scatter plots (See Figure 3.8, Figure 3.9, Figure 3.10, and Figure 3.11) describe these qualities and quantities.

It is clear in Figure 3.8 and Figure 3.9 that the orange nodes, which indicate the nodes from the schizophrenic group, are further from the origin than the blue nodes are. This indicates that the overall strength of the inhibitory connections in the slow 4 and slow 5 frequency bands are stronger in the schizophrenic group than they are in the control group. Notably, these plots and metrics do not contain any information about statistical significance of these differences. However, they do reflect the statistically significant findings presented in the square and circle plots from the previous sections (See: Figure 3.1, Figure 3.2, and Figure 3.4 through Figure 3.7), which clearly show that the schizophrenic group does indeed have an abundance of connections that are relatively more inhibitory than those observed in the control group. Some distinction can be made about excitatory connections in the slow 4 frequency band for a select few nodes (See Figure 3.10), namely the LaPFC_SN, LIns, RIns, RlPar_SN. However, these distinctions are not clear in the slow 5 frequency band, shown in Figure 3.11.

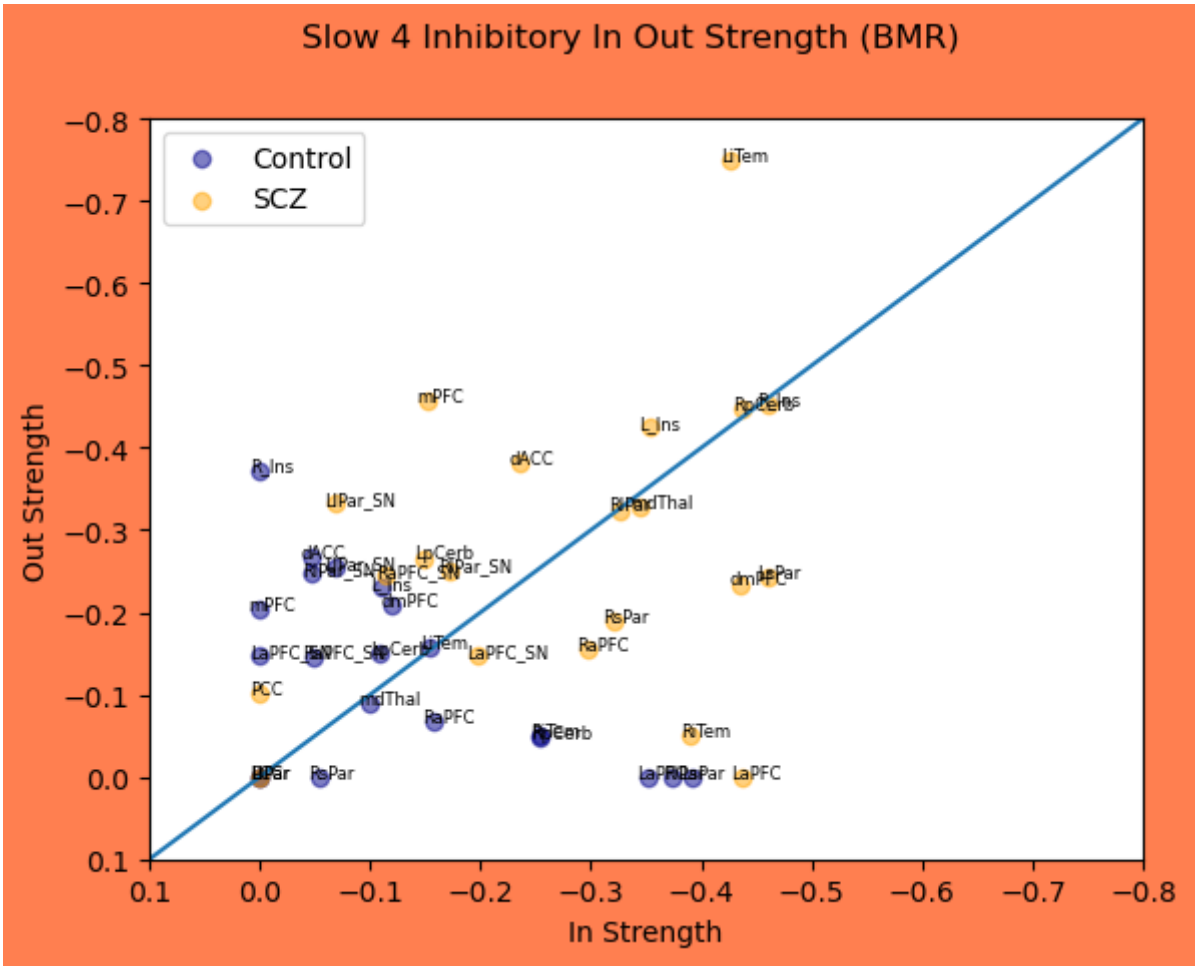

Figure 3.8.: Source-sink plot of inhibitory EC values for each node using posterior estimates from reduced second level models using information from the slow 4 frequency band.

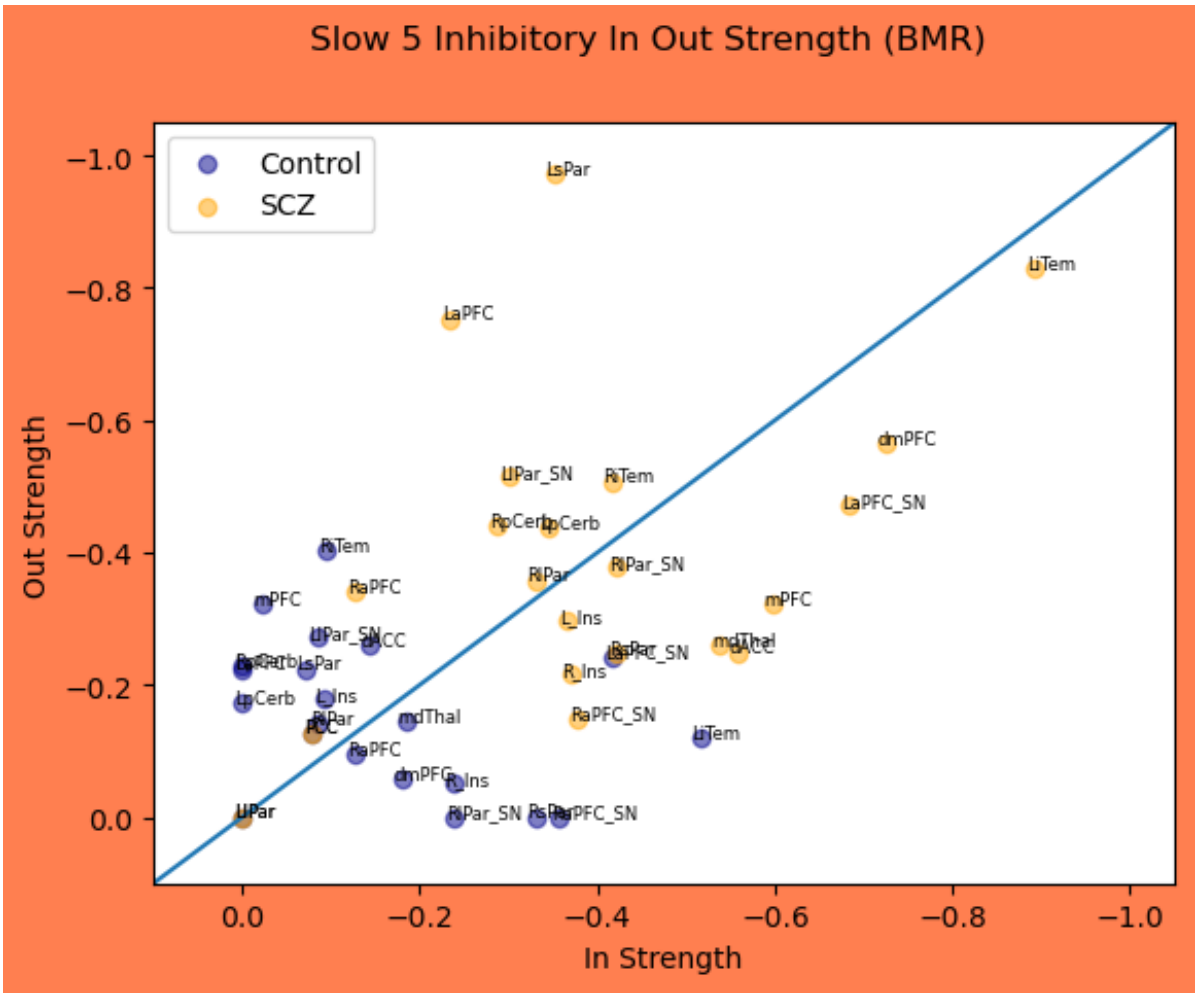

Figure 3.9.: Source-sink plot of inhibitory EC values for each node using posterior estimates from reduced second level models using information from the slow 5 frequency band.

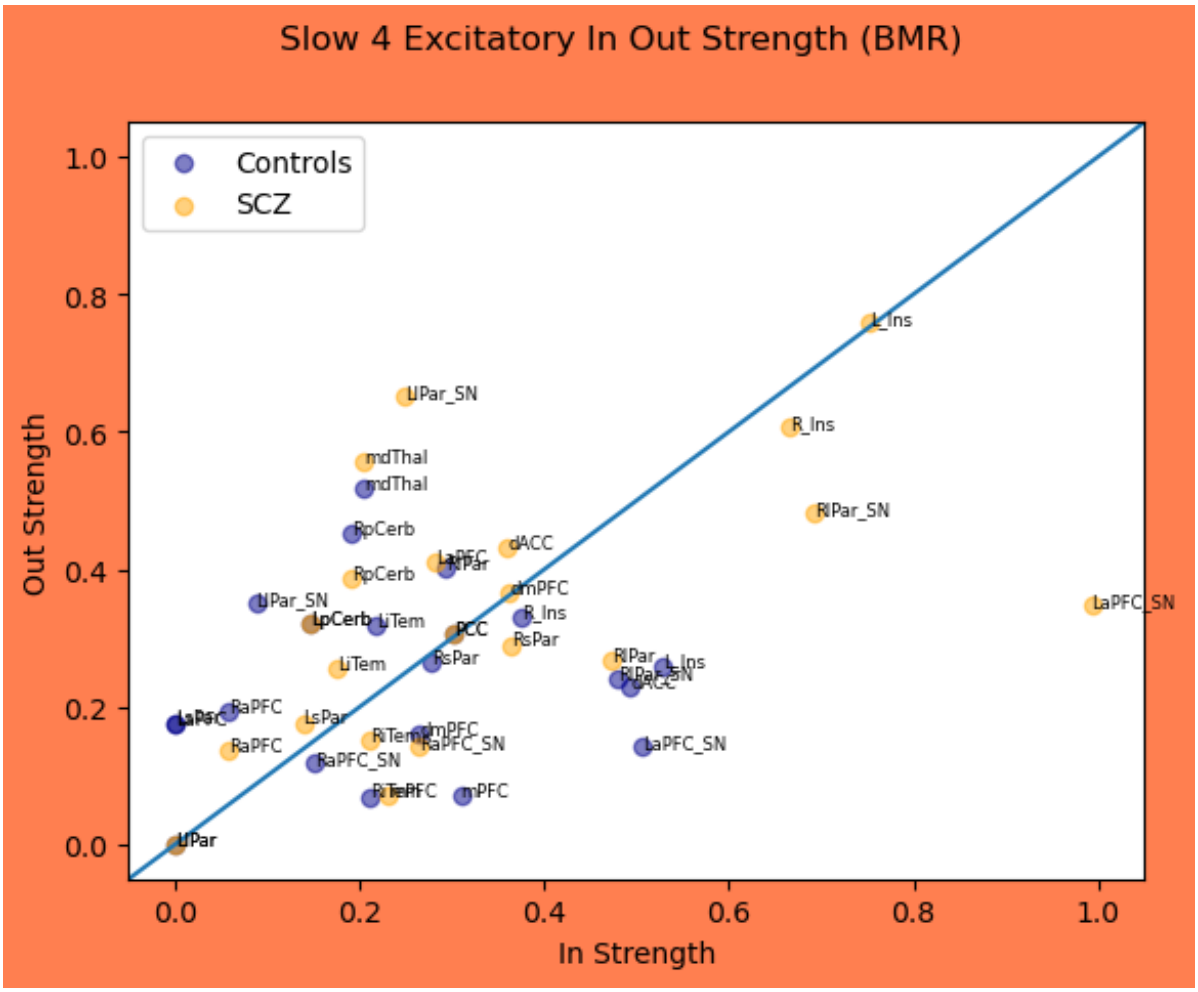

Figure 3.10.: Source-sink plot of exitatory EC values for each node using posterior estimates from reduced second level models using information from the slow 4 frequency band.

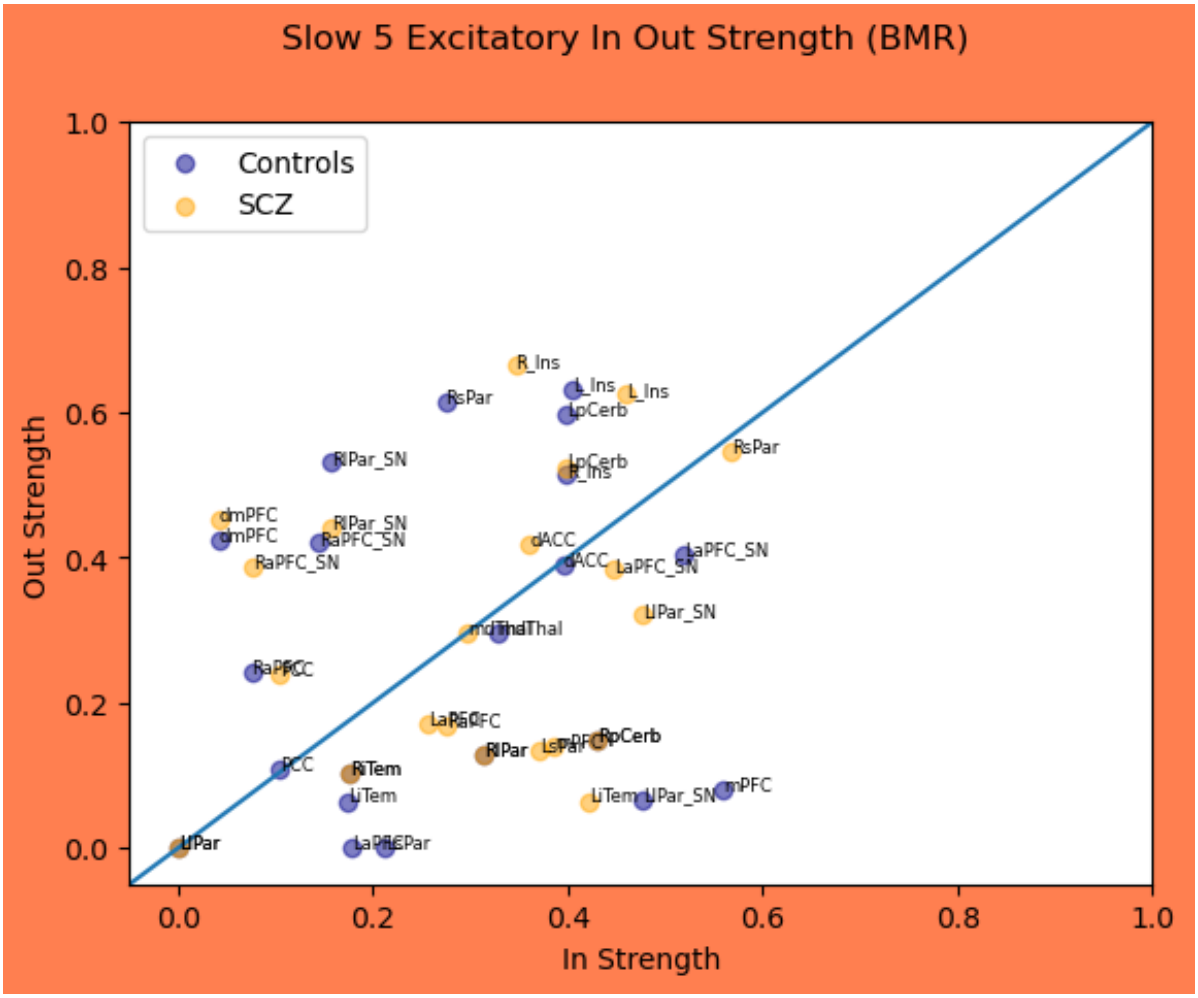

Figure 3.11.: Source-sink plot of excitatory EC values for each node using posterior estimates from reduced second level models using information from the slow 5 frequency band.

3.4. Differences in regional average Fractional Anisotropy

A one sided difference in means test was used to test for differences in the non-weigted and weighted regional average fractional anisotropies between the control and patient groups in the standard space defined by the O'muircheartaigh and Jbabdi [54] ICs, and to evaluate whether there was reduced FA in the white matter regions of the Talairach atlas. All of the p-values generated by these t-tests were subjected to false discovery rate (FDR) correction using the Benjamini-Hochberg method [10] as implemented via the **fdrcorrection** function from the statsmodels.stats.multitest Python package. The statistically significant results that remained after FDR correction are summarized and presented in tables in the following two subsections. Complete information on all of the tests are made available in tabular form in the supplementary materials.

3.4.1. O'muircheartaigh and Jbabdi ICs

In the series of tests comparing the non-weighted and weighted regional average fractional anisotropies within the O'muircheartaigh and Jbabdi IC space [54] between the groups, none of the 50 regions were found to have statistically significantly different average FAs after FDR correction. While it would be interesting to assess how white matter tract density in regions associated with prominent grey matter nuclei is altered in schizophrenia, we unfortunately are not able to derive any such conclusions from this study. However, we fortunately have the more standard Talairach atlas space analyses to fall back on to make conclusions about group differences in regional average FA in distributed regions of the brain. In future studies we may conduct probabilistic tractography with the control and patient data using a standard space such as FSL's [43] XTRACT space to assess differences in white matter density across predefined major white matter fibre tracts; this would additionally enable direct coupling of FA to EC information if we also included the GM independent components, i.e., seed regions, in the sp-DCMs instead of using the spherical ROIs that we use here. For now, we are limited to interpreting the statistically significant results that were generated by comparing regional average FAs within the WM ROIs of the Talairach atlas.

3.4.2. Talairach White Matter Regions

The white matter regions of the Talairach atlas that were statistically significantly different between the groups after FDR correction are the regions with indices: 14, 20, 24, 28, 51, 52, 134, 253, 308, 486, 929, and 1051, indicating that 12 of the 110 t-tests yielded statistically significant results after FDR correction [10]. In order (and as shown in Figure 3.12), these indices refer to the following regions: Left Inferior Temporal Gyrus, Right Inferior Temporal Gyrus, Left Middle Temporal Gyrus, Right Middle Temporal Gyrus, Left Temporal Sub-gyral WM, Right Temporal Sub-gyral WM, Right Parahippocampal Gyrus, Right Lingual Gyrus of the Occipital Lobe, Left Middle Occipital Gyrus, Right Cuneus of the Occipital Cortex, Left Parietal Supramarginal Gyrus, and Left Frontal Paracentral Lobule. All of these findings are summarized in Figure 3.12, which includes the difference in regional average fractional

anisotropy, the corrected and uncorrected p-values, and the one-sided confidence interval associated with the t-tests used. The complete information for all 110 tests can be found in the supplementary materials.

LABEL ID	REGION NAME	ΔFDR P-VAL	95% CI	P-VAL
14	Left Cerebrum.Temporal Lobe.Inferior Temporal Gyrus	0.0182	0.0309	0.0092	0.0006
20	Right Cerebrum.Temporal Lobe.Inferior Temporal Gyrus	0.0128	0.0362	0.0053	0.0030
24	Left Cerebrum.Temporal Lobe.Middle Temporal Gyrus	0.0134	0.0352	0.0057	0.0023
28	Right Cerebrum.Temporal Lobe.Middle Temporal Gyrus	0.0113	0.0347	0.0052	0.0013
51	Left Cerebrum.Temporal Lobe.Sub-Gyral	0.0131	0.0352	0.0055	0.0026
52	Right Cerebrum.Temporal Lobe.Sub-Gyral	0.0123	0.0480	0.0045	0.0052
134	Right Cerebrum.Limbic Lobe.Parahippocampal Gyrus	0.0114	0.0367	0.0046	0.0033
253	Right Cerebrum.Occipital Lobe.Lingual Gyrus	0.0169	0.0316	0.0082	0.0009
308	Left Cerebrum.Occipital Lobe.Middle Occipital Gyrus	0.0160	0.0347	0.0071	0.0018
486	Right Cerebrum.Occipital Lobe.Cuneus	0.0167	0.0239	0.0091	0.0002
929	Left Cerebrum.Parietal Lobe.Supramarginal Gyrus	0.0172	0.0386	0.0067	0.0039
1051	Left Cerebrum.Frontal Lobe.Paracentral Lobule	0.0197	0.0347	0.0086	0.0019

Figure 3.12.: White matter regions of the Talairach atlas with statistically significantly lower average fractional anisotropies in the schizophrenic group compared to the control group.

These results clearly indicate that the regional average FA of the inferior, middle, and sub-gyral temporal lobe is generally decreased in the schizophrenic group, and that other cortical regions in the frontal, parietal, and occipital lobes exhibit reduced average FA in select nuclei. These findings are consistent with findings from existing studies, which will be the subject of further elaboration in the ensuing discussion chapter.

3.5. Differences in cognitive scores

A multivariate regression analysis was conducted for each of the following cognitive scores to test for differences between the control and patient groups while controlling for the subject's sex. The cognitive scores tested were: Auditory reaction time for and number of correct responses across all tasks of those types in the Seidmann auditory continous performance test (acpt) [66] [65]; fluid and crystallized cognition scores, which are composite scores of NIH-Toolbox measures [88] [81] [82] [37]; the HCP Lifespan measures [33] [32], which includes delayed discounting tasks of which we will use two specific metrics; and the number of correct responses and reaction time for said correct responses in the Penn emotion recognition task. More complete details about the cognitive scores collected in this data-set are available on

pages 7-8 in the HCP-EP release manual[2]. All of the results of these multivariate regressions are summarized in tables in the general addenda (See: Figure A.1 through Figure A.10). These results will be summarized and the tables referred to in the following subsections.

3.5.1. Auditory Processing

The first multivariate regression models used to test for differences in auditory processing performance included only the subject's sex and group belongingness (i.e., whether the subject was in the control or non-affective psychosis group) as covariates. As can be seen in the regression tables, both in the case of hit rate and reaction time, both the coefficients associated with sex and group belongingness were statistically significant at the 5% level. This would indicate that in the 'hit rate' category, the female subjects performed 4.5 points worse on average than the males, and that the patients in the schizophrenic group performed 11.87 points worse on average than the controls. This would also indicate that in the 'response time' category the females responded approximate 35*ms* slower than the males on average, and the non-affective psychosis group responded 56*ms* slower than the controls on average. Given that there is no obvious reason that either sex should perform worse on this task than the other, I included an interaction term of sex and diagnosis to investigate this oddity. The results of these regressions with interaction terms are displayed in a second set of tables (See: Figure A.1 Figure A.2 Figure A.3 Figure A.4), and indicate that sex alone is not a statistically significant covariate in the model. Rather, the interaction term indicates that in terms of 'hit rate' the schizophrenic group performed approximately 11.4 points lower than the control group on average and that there was no difference in performance between the sexes. For the response time, the linear sex term was also statistically insignificant when the interaction was included. Additionally, the linear diagnosis variable became statistically insignificant with a coeffient of 30*ms* (slower than the controls) and p-value of 0.14. However, the interaction term is statistically significant with a coefficient of 66.11*ms* and p-value of 0.044. These metrics indicate that the females in the schizophrenic group responded 96.34*ms* slower on average than those subjects in the control group, which is statistically significantly slower. This was notably the driving factor in the original models that indicated that sex was a statistically significant covariate itself.

3.5.2. Delayed Discounting Task

The delayed discounting tasks used for the analyses in this work are the 'deldisk01_sv_10yr_40000' and 'deldisk01_sv_6mo_40000', which indicate the present value evaluation of $40,000 at the time intervals of 10 years from now and 6 months from now, respectively. As can be seen in the respective regression tables (See: Figure A.5 Figure A.6), the schizophrenic group evaluated this sum as being worth statistically significantly less in both cases in comparison to their control counterparts. In the case of the 10 year delayed reward, the control group evaluated $40,000 10 years from now as being worth roughly $14,800 today, whereas the

[2] https://www.humanconnectome.org/storage/app/media/documentation/HCP-EP1.1/HCP-EP_Release_1.1_Manual.pdf

schizophrenic group evaluated this sum as being worth $5,927.43 less than that on average (p=0.009) for a total of $8,872.57. This is roughly 60% of the value that the controls give to $40,000 10 years down the road. For the 6 month delayed discount task, the control group evaluated $40,000 as being worth approximately $33,480 on average, and the schizophrenic group evaluate it as being worth $6,976.41 less than that on average (p=0.001) for a total of $26,503.59, which is 79.16% of the value that the control group gave to receiving the delayed sum. This seems to be indicative of the schizophrenic group evaluating large rewards as being less valuable as time goes on in comparison to their control group counterparts.

3.5.3. Fluid and Crystallized Intelligence

In terms of both fluid and crystallized intelligence, which are quantified as composite scores from the NIH Toolbox Cognitive Battery (NIH-CB), the schizophrenic group performed worse on average compared to the controls. The difference in scores in the fluid intelligence category was 15.8357 on average, yielding a p-value <0.001; This is equivalent to an approximate reduction in fluid intelligence score of 14.12% in the schizophrenic group. For the crystallized cognition variable, the difference was 8.2293 on average, which also yields a p-value <0.001, and is indicative of an approximate 7.46% reduction in crystallized intelligence score on average in the schizophrenic group compared to controls. These results are also displayed in tables in the general addenda (See: Figure A.7 Figure A.8)

3.5.4. Emotion Recognition

In the Penn emotion recognition tasks[3], the average number of correct responses and the average response times for those correct responses were statistically significantly different between the control and patients groups, and the sex covariate was statistically insignificant in both models. With respect to the number of correct responses out of 40, the controls answered 35.54 correctly on average while the schizophrenic group answered only 33.76 correctly on average, which is a difference of 1.78 points yielding a p-value of 0.001. In terms of response times, the control group took approximately 1.825s on average to answer correctly, whereas the schizophrenic group took 443.43ms longer on average (p-val<0.001) for a total of 2.27s on average to answer correctly. This increase in response time indicates that the schizophrenic group was 24.29% slower to respond on average than the control group in the emotion recognition tasks. The regression tables for these variables can be found in Figure A.9 and Figure A.10

3.6. Canonical Variate Analysis

The canonical variate analyses serve to assess the relationship between the effective connectivity values and cognitive and clinical scores. An independent analysis was conducted for each frequency band onto the cognitive and clinical scores, resulting in a total of 4 models.

[3] `https://nda.nih.gov/data_structure.html?short_name=er4001`

The principal canonical vectors and variates of those models are reported here. The protocols for selecting the features for these models is described in the corresponding methods section (2.9); the processes were conducted to best reflect the practices employed in the publication of Zarghami et al., 2023 [86].

In the model comparing slow 5 frequency band EC to the composite cognitive scores, the self inhibition of the LiTem, EC from the LpCerb to RpCerb, and EC from the PCC to LiTem were the ones that best explained the variance in the composite emotion recognition score and averaged fluid and crystallized cognition scores (Figure 3.13; Chi=53.807, $p<0.001$, $r=0.794$). In the slow 4 band EC to cognitive score model, the connections that were chosen are the LIns to LlPar_SN, LaPFC_SN to RlPar, and the RlPar self inhibition (Figure 3.16; Chi=53.517, $p<0.001$, $r=0.813$). It should be noted that these models are mostly weighted by the emotion recognition composite score, which outweighs the fluid and crystallized cognition composite score by a factor of approximately 9 in both slow 5 and slow 4 models.

In the slow 5 to clinical score model, the EC features that were chosen are the PCC to RlPar, the RlPar_SN self inhibition, and the dACC to LaPFC_SN EC (Figure 3.19; Chi=59.845, $p<0.001$, $r=0.830$), indicating the importance of the fronto-parietal network in the explanatory power of the variance in PANSS general and PANSS positive scores, and to some degree the variance in the PANSS negative scores. Figure 3.22 indicates that the following connections from the slow 4 frequency band models provide the largest explanatory power to the variance in the PANSS positive and PANSS negative clinical scores: RiTem to RlPar, the dmPFC self inhibition, and the mPFC to mdThal connection (Chi=44.181, $p<0.001$, $r=0.781$).

Notably, the second canonical vectors were statistically significant for each model, however, due to limited space they are not shown in the body of the text but are included in a supplementary materials document. Additionally, it is interesting to note that the regions being chosen by the CVA models are consistently among those regions that exhibit the most altered EC profiles as shown in the source-sink profile section, and are also the regions that have exhibited reduced regional average FA in the schizophrenic group; this is true even though the differences in these metrics between the groups is not a factor that is considered by the CVA models. More attention to the interpretation and contextualization of these results is given in the corresponding section of the discussion.

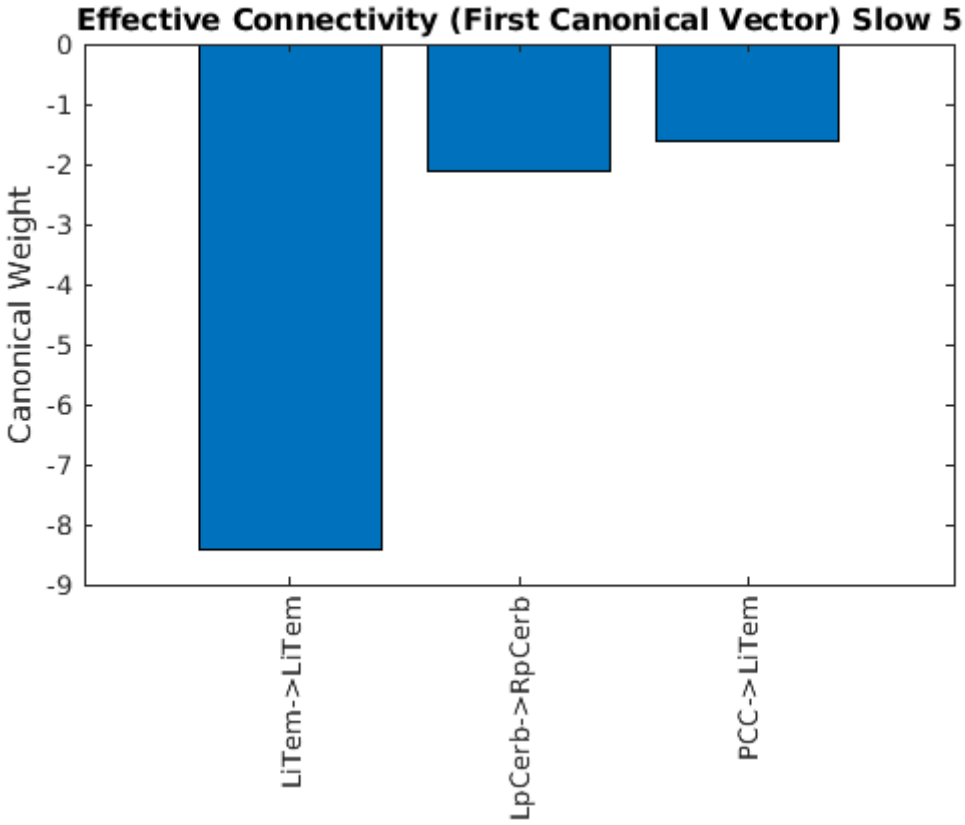

Figure 3.13.: Node to node connections whose EC values best describe the variance in emotion recognition and fluid and crystallized cognition task scores. Chi: 53.807, r:0.794, p-val:<0.001

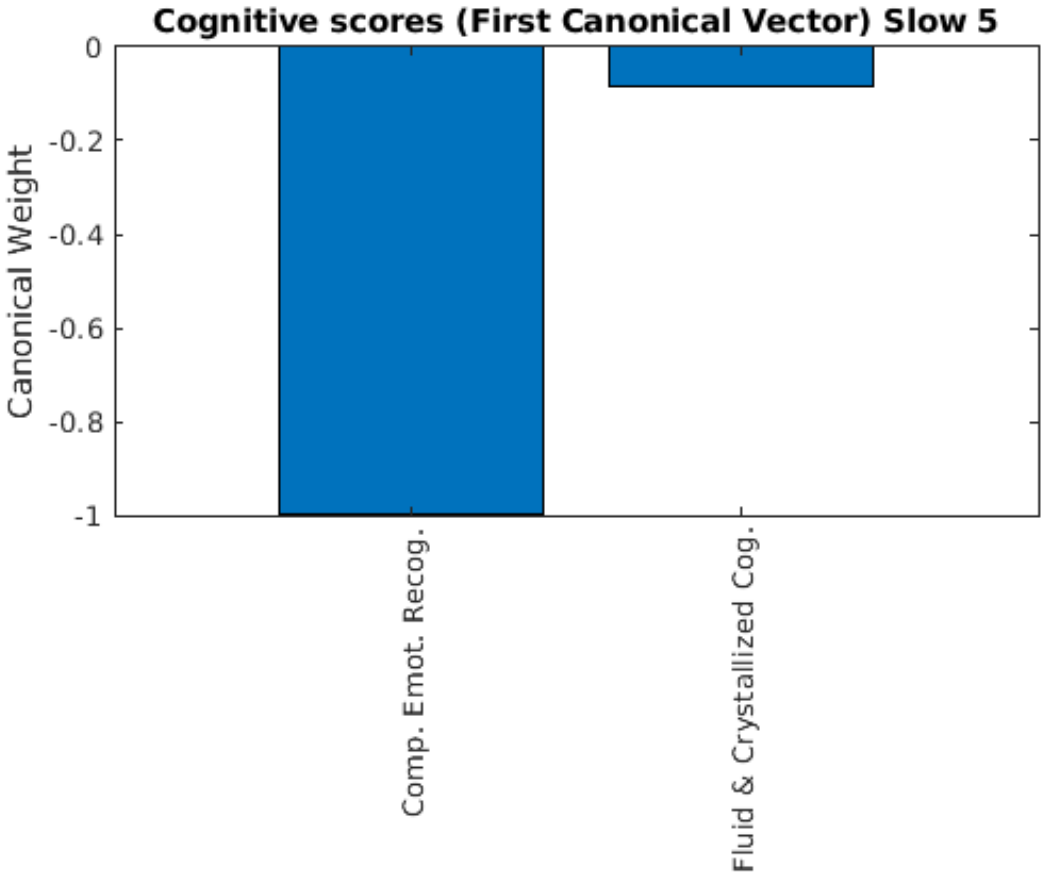

Figure 3.14.: Canonical weights of cognitive scores from the first canonical vector contributing to the slow 5 model

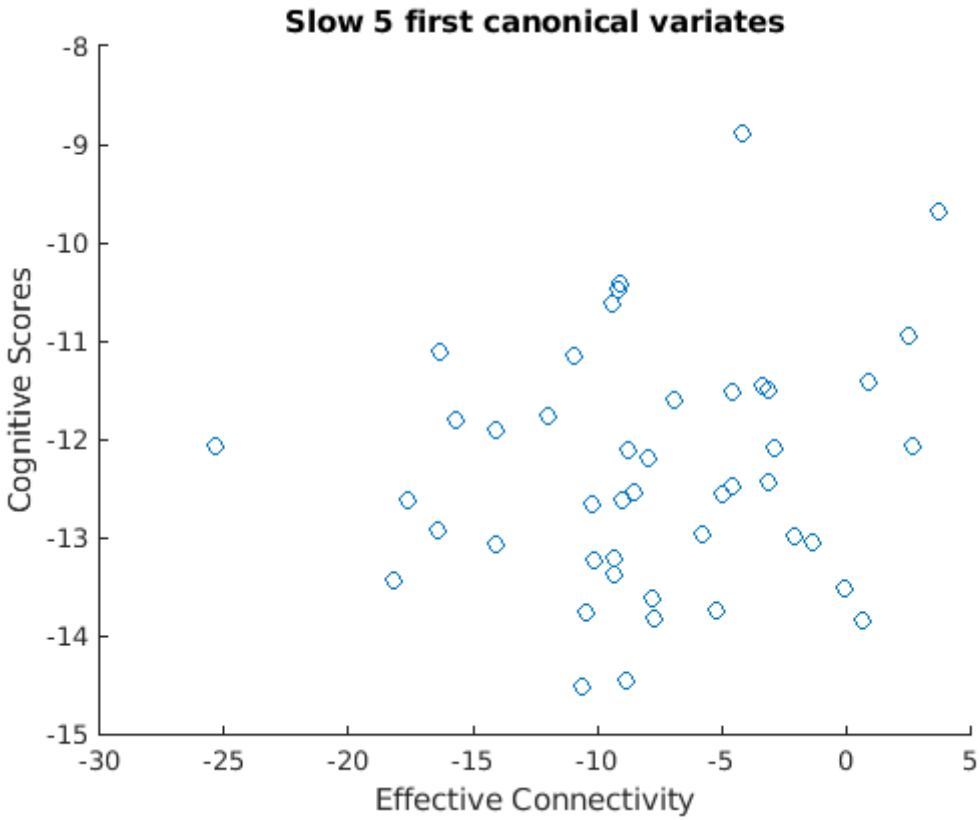

Figure 3.15.: Correlation of the canonical variates from the first canonical vector of the slow 5 model using cognitive scores as dependent variables

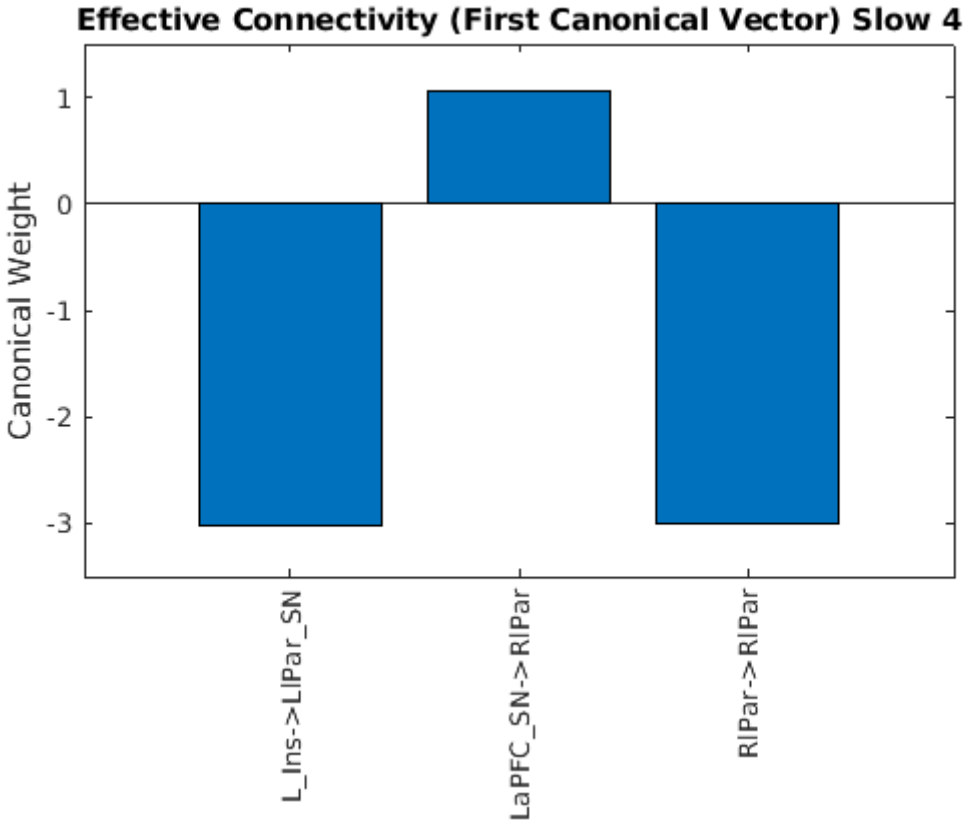

Figure 3.16.: Node to node connections whose EC values best describe the variance in emotion recognition and fluid and crystallized cognition task scores in the principal canonical vector of the slow 4 model. Chi:53.517, r:0.813, p-val:<0.001

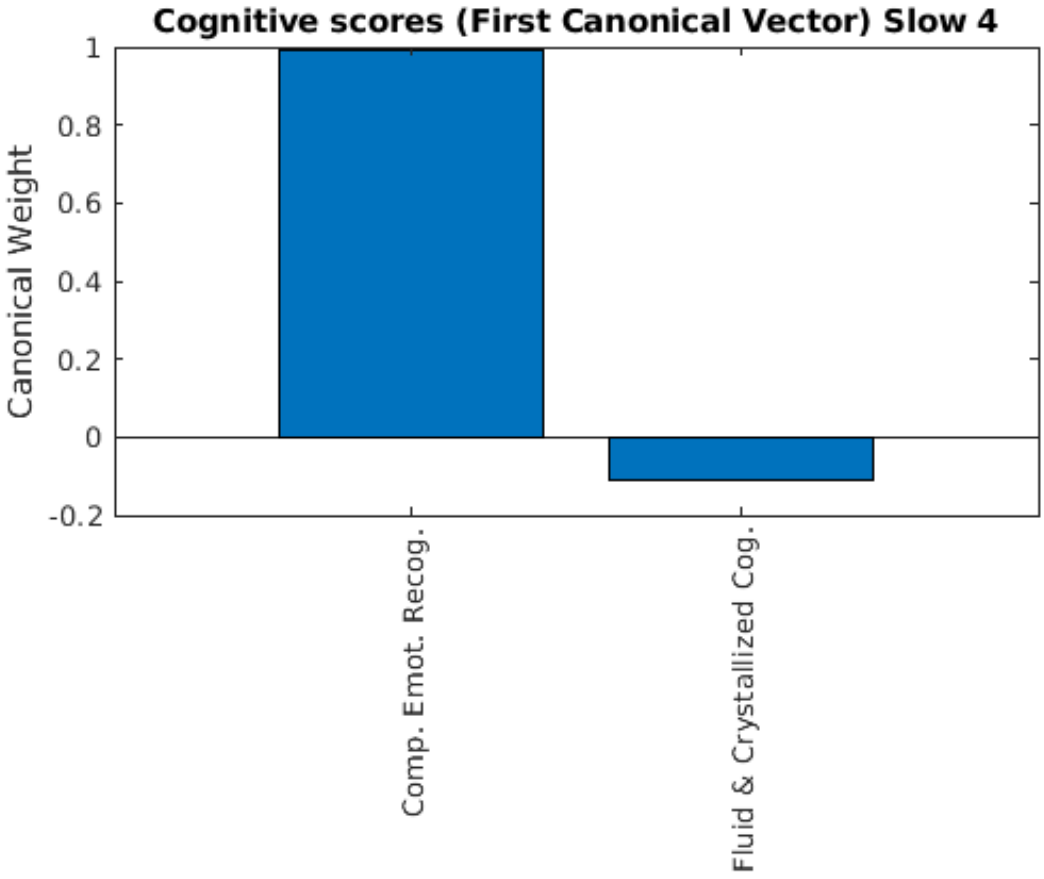

Figure 3.17.: Canonical weights of cognitive scores from the first canonical vector contributing to the slow 4 model

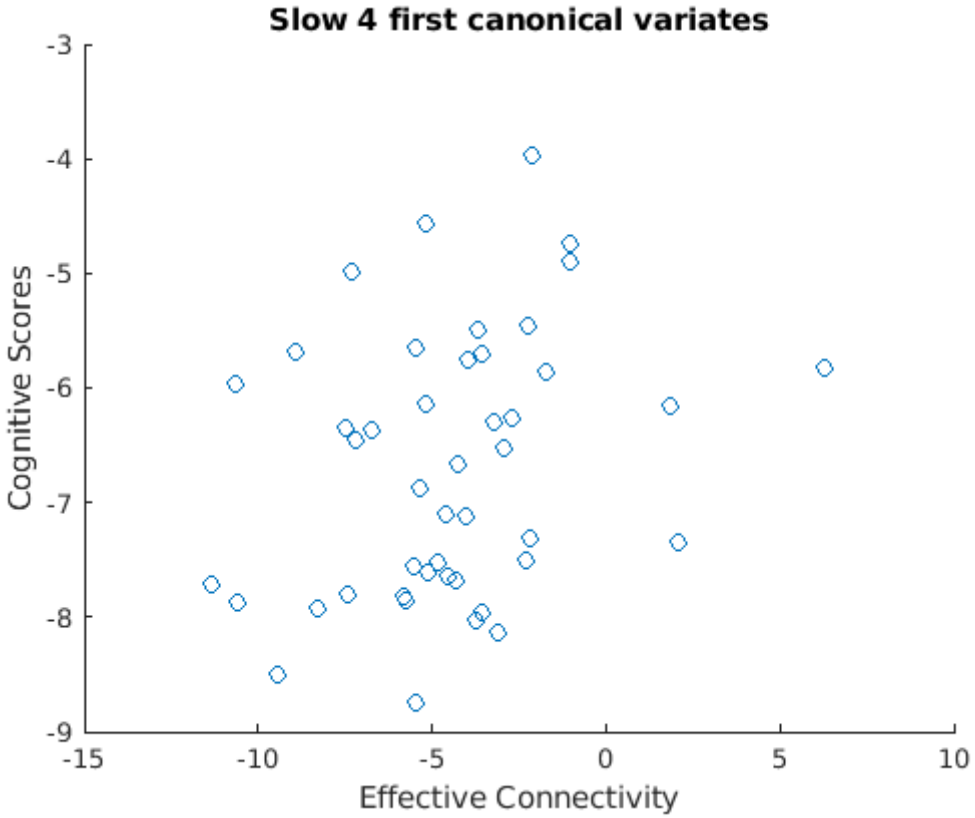

Figure 3.18.: Correlation of the canonical variates from the first canonical vector of the slow 4 model using cognitive scores as dependent variables

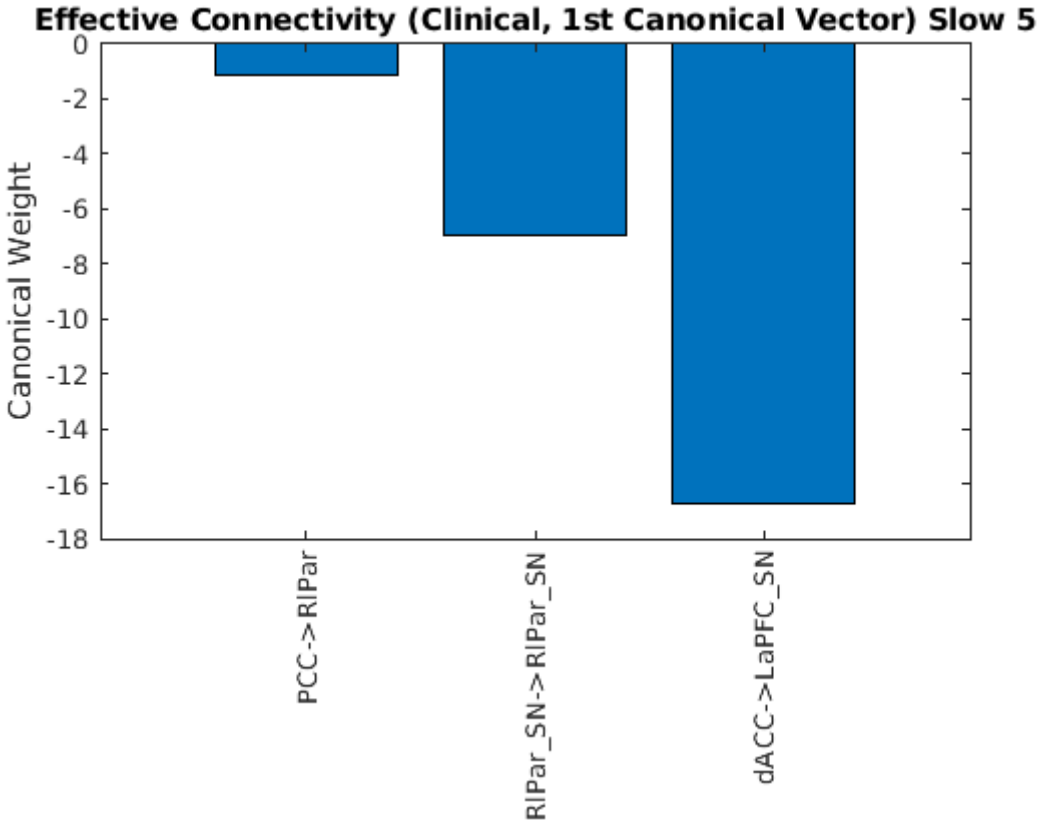

Figure 3.19.: Node to node connections whose EC values best described the variance in PANSS general, positive, and negative scores in the principal canonical vector of the slow 5 clinical model. Chi:59.845, r:0.830, p-val:<0.001

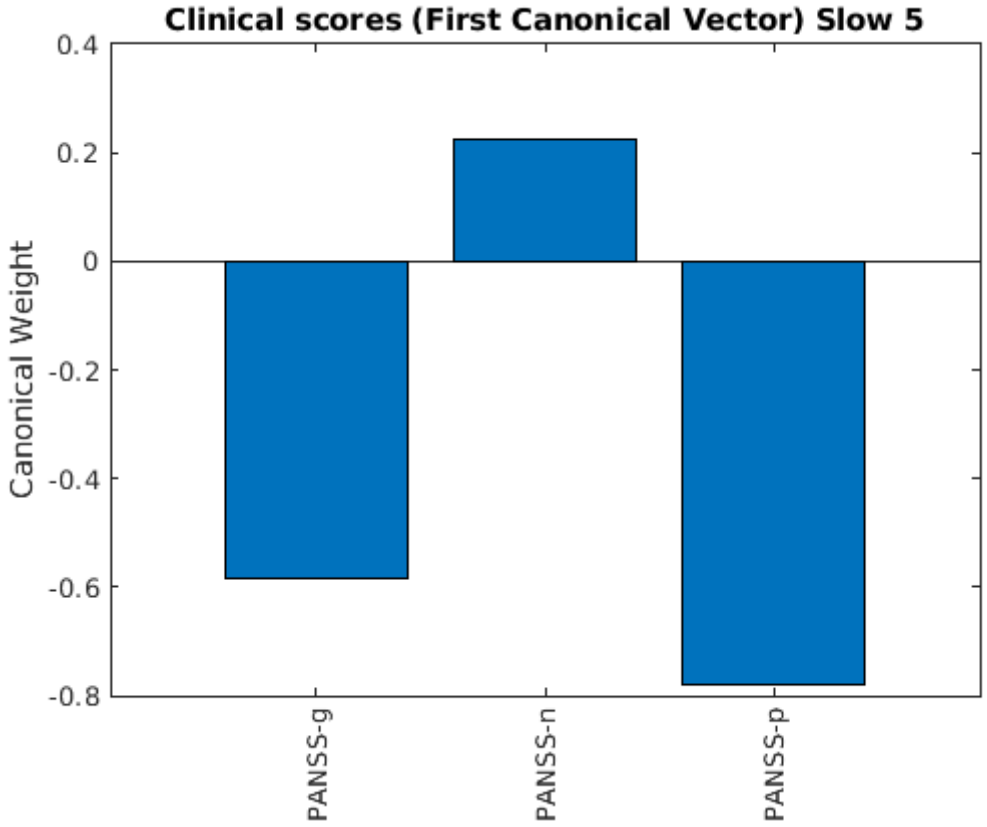

Figure 3.20.: Canonical weights of clinical scores from the first canonical vector contributing to the slow 5 clinical model

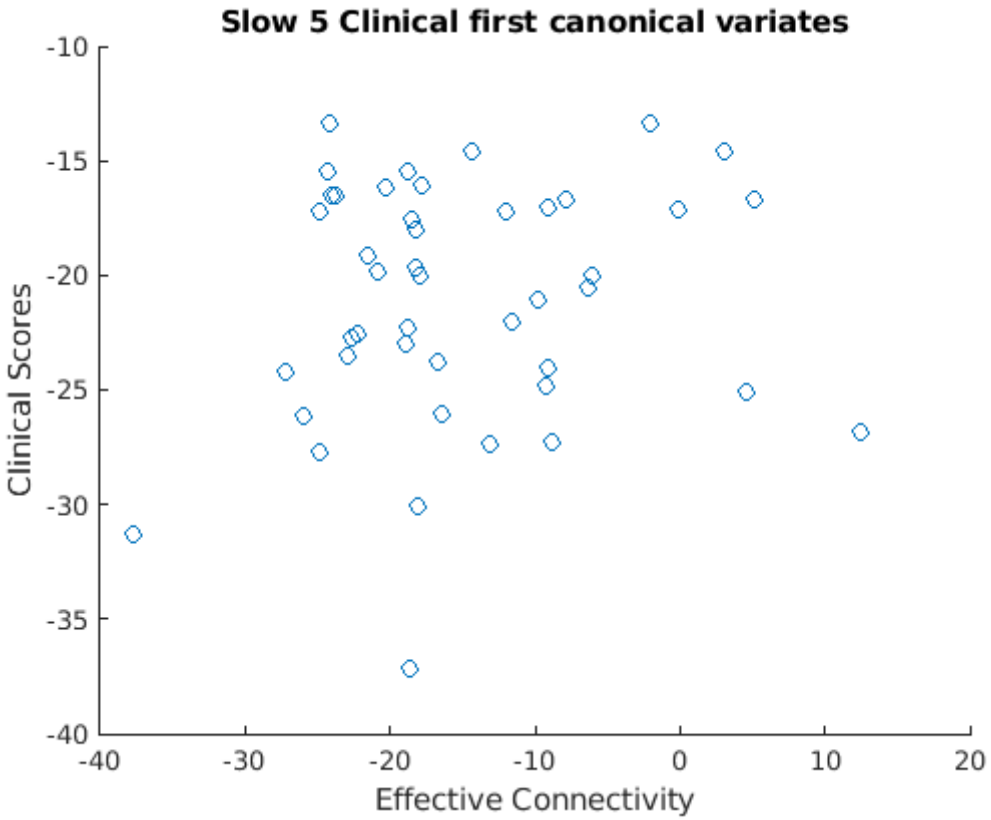

Figure 3.21.: Correlation of the canonical variates from the first canonical vector of the slow 5 model using clinical scores as dependent variables

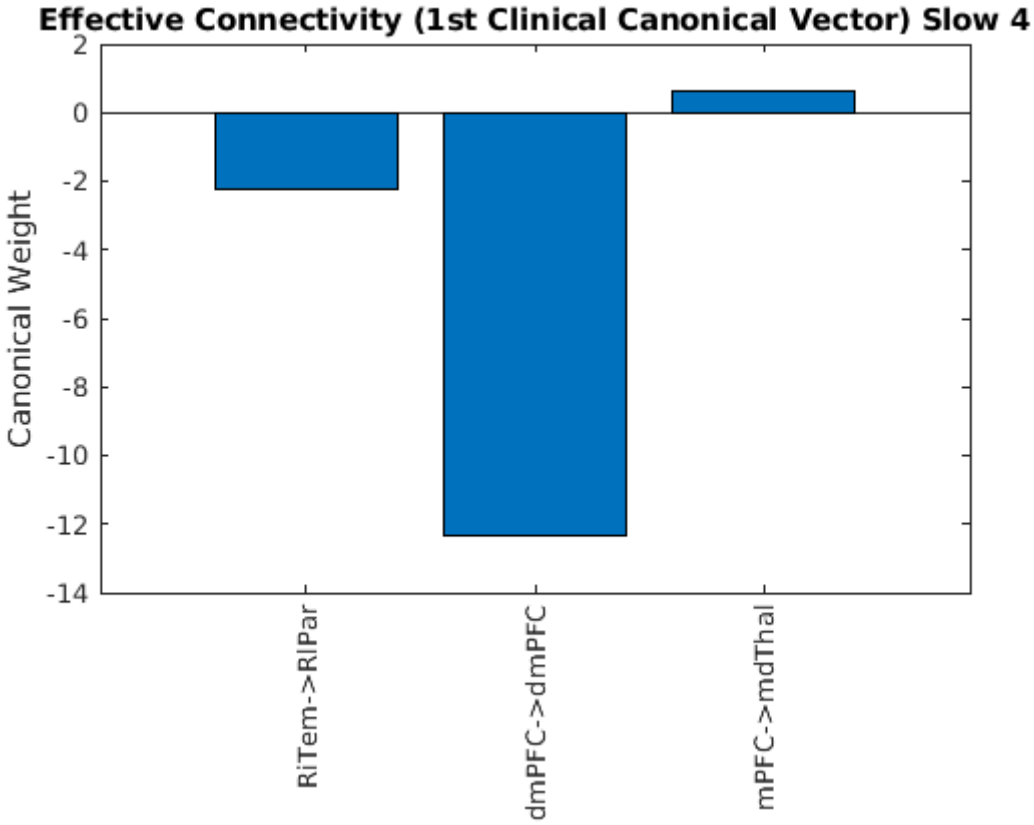

Figure 3.22.: Node to node connections whose EC values best described the variance in PANSS positive and negative scores in the principal canonical vector of the slow 4 clinical model. Chi:44.181, r:0.781, p-val:<0.001

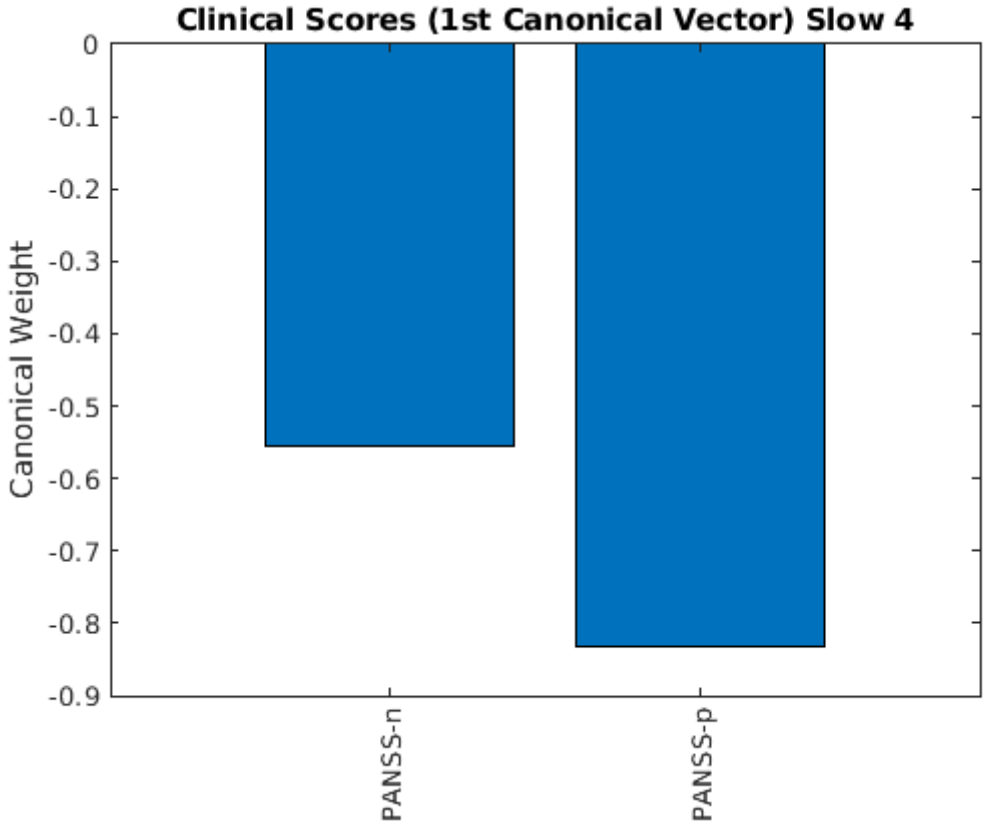

Figure 3.23.: Canonical weights of clinical scores from the first canonical vector contributing to the slow 4 clinical model

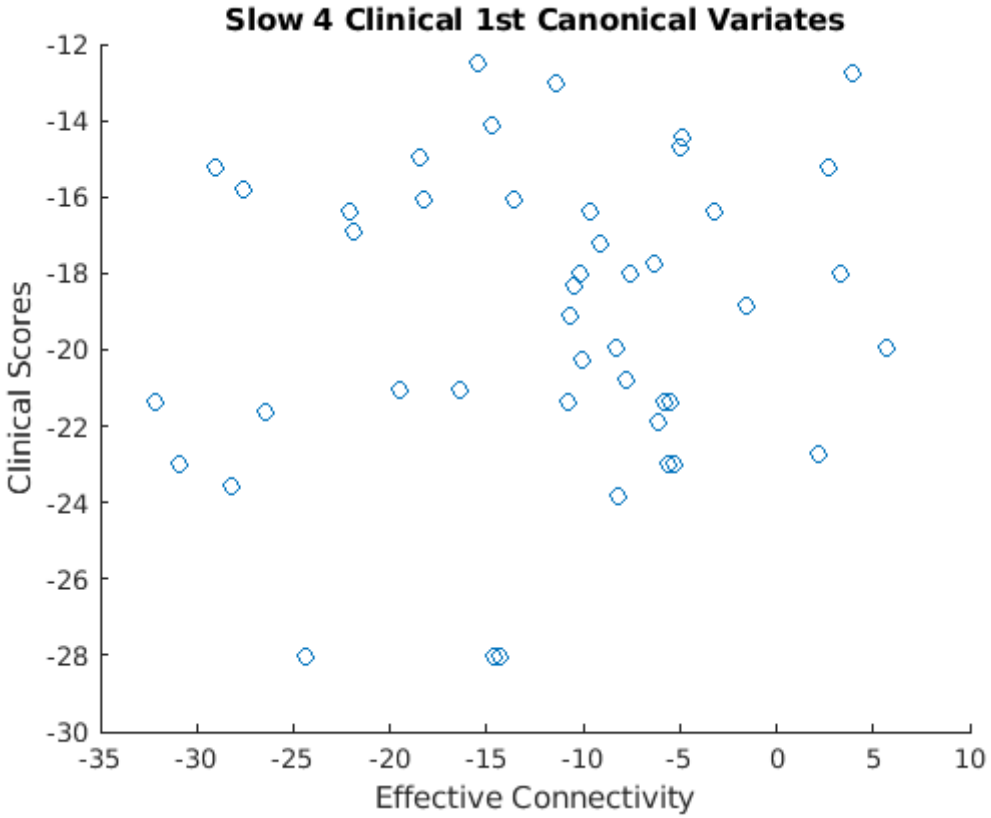

Figure 3.24.: Correlation of the canonical variates from the first canonical vector of the slow 4 model using clinical scores as dependent variables

3.7. Summary of the results

Posterior expectations of intrinsic effective connectivity parameters were compared to their posterior variances as estimated by the Parametric Empirical Bayes (PEB) models that underwent Bayesian Model Reduction (BMR). The expected values of the differences in EC strength between groups that had magnitudes exceeding two times the associated standard deviation were deemed to be statistically significant. Those statistically significant differences are visualized in the circle plots of section 3.2 and in section 3.1.1, specifically in Figure 3.2. The proportion of significantly altered connections within and between the three networks that were modeled is described in section 3.1.2. It is clear that there is a general tendency towards greater inhibition in the node to node connections in the slow 5 frequency band for the group of subjects with schizophrenia, where the greatest proportions of altered EC existing within the reciprocal connections of the DMN and CEN and in the connections from the CEN to the SN. In the slow 4 band there is both increased inhibition in some node to node connections, and increased excitation in others with the majority of altered connections being present within the SN and between the CEN and SN.

The one-sided t-tests conducted to test for reduced weighted and non-weighted average FA values in the white matter regions of the O'muircheartaigh and Jbabdi ICs [54] were all statistically insignificant. Of the 110 one-sided t-tests that were conducted to test whether FA values were reduced in the schizophrenic group in the white matter regions of the Talairach atlas, 12 were statistically significant after FDR correction [10]. The Talairach regions where the schizophrenic group displayed statistically significantly reduced average FA are listed in section 3.5.2 and Figure 3.12. Namely, there were observed reductions in regional average FA in the middle and inferior bilateral temporal gyri and respective sub-gyral WM, the left frontal paracentral lobule, the left parietal supramarginal gyrus, right occipital cuneus and lingual gyrus, left middle occipital gyrus, and the right parahippocampal gyrus.

For the cognitive scores, the schizophrenic group scored lower on average across all metrics used in this study, specifically in auditory processing, delayed discounting, fluid and crystallized cognition, and emotion recognition. How this relates to altered effective connectivity was investigated via canonical variate analyses.

The series of four canonical variate analyses revealed that in the slow 5 frequency band, altered intra-DMN connectivity was best at explaining the variance in altered emotion recognition and to some extent fluid and crystallized cognition, with the self-inhibition of the Left inferior Temporal Cortex (LiTem) being the strongest predictor of the cognitive scores in the schizophrenic group. This connection was followed by the projection from the LpCerb to the RpCerb and the projection from the PCC to the LiTem. See Figure 3.13 - Figure 3.15. In the slow 4 band, select connections from the SN to the DMN and the self inhibition of the RlPar were found to have the strongest explanatory power of the variance in emotion recognition and fluid and crystallized cognitive capacities in the schizophrenic group. Specifically, strength of the EC from the LIns to the LlPar_SN and the self inhibition of the RlPar were the strongest predictors, followed by the projection from the LaPFC_SN to the RlPar See Figure 3.16 - Figure 3.18.

In the slow 5 frequency band, variance in clinical scores was best described by intra-SN

connectivity, specifically from the dACC to the LaPFC_SN and the self inhibition of the RlPar_SN. Additionally, the connectivity from the mPFC to the mdThal was included in the feature selection, and constitutes an intra-DMN connection. The strength of effective connectivity of those connections best described the variability in PANSS general and PANSS positive scores; See Figure 3.19 - Figure 3.21. In the slow 4 frequency band, variance in PANSS positive and PANSS negative scores were best explained by the self inhibition of the dmPFC, a node of the CEN, followed by the projection of the RiTem to the RlPar and the projection from the mPFC to the mdThal, which are both intra DMN connections; notably, the self-inhbition of the dmPFC greatly outweighed the contribution of the other connections in this model. See Figure 3.22 - Figure 3.24.

4. Discussion

In this chapter, the results of this thesis will be contextualized with respect to existing findings from other studies that describe altered effective connectivity, fractional anisotropy, and the relationship between effective connectivity and disease severity in patients with schizophrenia spectrum disorders. This will be done by reporting the primary results of a selection of recent studies that have tested similar hypotheses using similar methods e.g., Zarghami et al., 2023 [86] and Zhou et al., 2018 [89]. Given that some studies use different sets of nodes and different definitions for network belongingness of certain nodes, the comparison may not always be one to one. However, it will be shown in the following sections that there are still several results of this thesis that are generally consistent with existing findings with respect to altered EC, FA, and correlations between EC and cognitive and clinical scores within the patient group. After these points have been addressed, the relevance and limitations of this thesis will be described, and a statement on the most logical next steps for future works will be made.

4.1. Contextualizing the differences in Effective Connectivity (EC)

Generally, the studies whose results are reported here indicate significant alterations in EC in the fronto-parietal-temporal cortices as well as in subcortical structures such as the cingulum and parahippocampal gyri. Some examples include: Deserno et al., 2012 that reports "...evidence for disordered prefrontal to parietal EC in schizophrenia using DCM." [15], which is consistent with the nodes found to be implicated in the CVA on the cognitive scores using slow 4 frequency band information in this study (Figure 3.16); In the Deserno et al., 2012 paper, the authors cite Rihs et al., 2013 "...who also found in a 22g11.2 [deletion] cohort an enhanced N1 [, a visually evoked potential,] component that was explained by a greater activation in the mPFC and dACC [62]." [15]. In this study, connections involving the dACC and mPFC were both found to be in the set of strongest predictors of clinical symptom severity, specifically with respect to PANSS positive, negative, and general scores (Figure 3.19 & Figure 3.22).

In Zhou et al., 2018 a conclusion was "...that intrinsic and extrinsic connections in three key large scale brain networks, especially those involving the prefrontal cortex, were altered in schizophrenia." [89]. In this study, the prefrontal cortex was selected as one of the best nodes in three of the four CVA models, and was either a source or target in 4 out of the 12 most strongly implicated connections. In Zarghami et al., 2023 the primary findings were that "...a remarkable one third of effective connections (among the subnetworks) of the Cognitive Control network have been pathologically modulated in schizophrenia [and

that] further dysconnection was identified in the visual network, default mode network, and somatomotor network with 24%, 20%, and 11% of their connections altered in schizophrenia, respectively." [86]. Three of the nodes in this study that are among the most strongly implicated in the CVA models generated here, namely the LIns, RlPar, and LiTem are nodes that exist within the cognitive control network as it is defined in the work of Zarghami et al., 2023 (See their Table 2) [86]. While this study does not model the somatomotor network, it does take into consideration nodes that are considered to belong to the DMN and visual network as Zarghami et al., define them [86]. Namely, the anterior cingulate cortex and PCC were defined as belonging to the DMN in the Zarghami et al., paper [86]. These cingulate nodes were among the nodes in the connections that best described the alterations in either cognitive or clinical scores in the CVA models generated in this thesis (See Figure 3.19 and Figure 3.13). While the nodes of the visual network were not modeled in the sp-DCMs that defined the EC values, it was found in this study that there was reduced regional average FA in the patient group in the cuneus, middle temporal gyri, and lingual gyrus, which are all nodes of the visual network in the Zarghami et al., 2023 publication [86].

4.2. Contextualizing the differences in Fractional Anisotropy (FA)

This study indicates that there are statistically significant differences in regional average Fractional Anisotropy (FA) in distributed regions of the brain. Specifically, in the patient group there is reduced average FA in: the inferior and middle temporal gyri and temporal sub-gyral white matter, the right parahippocampal gyrus, the left middle occipital gyrus, the right occipital cuneus and lingual gyrus, the supramarginal gyrus of the parietal lobe, and the left paracentral lobule of the frontal lobe. These results are displayed in Figure 3.12.

These results are consistent with existing findings that describe similar distributed reductions in fractional anisotropy. For example, Ardekani et al., 2003 found "...FA was lower for patients in the corpus callosum, left superior temporal gyrus, parahippocampal gyri, middle temporal gyri, inferior parietal gyri, medial occipital lobe, and the deep frontal perigenual region" [6]. This study found reduced average FA in the right parahippocampal gyrus, bilateral middle temporal gyri, left parietal supramarginal gyrus, left medial occipital lobe, and left paracentral lobule of the frontal gyrus, which is mostly consistent with the results published in Ardekani et al., 2003 [6]. Ardekani et al., 2003 also cite "Lim et al., [who] found widespread reductions in prefrontal and parieto-occipital WM regions in schizophrenia" [50]. This study found reduced average FA in the right occipital lingual gyrus and cuneus, left parietal supramarginal gyrus, left middle occipital gyrus, and left frontal paracentral lobule.

Yao et al., 2013 state that "consistent FA reductions in the WM of the right deep frontal and left deep temporal lobes were identified in all first episode psychosis patients relative to healthy controls...[and]...current findings provide evidence confirming the lack of connection in the fronto-limbic circuitry at the early stages of schizophrenia" [85]. This study indicated bilateral reductions in average FA in the inferior and middle temporal gyri as well as in the sub-gyral WM of the temporal lobes; more attention will be paid to their statement about reduced connectivity in fronto-limbic circuitry in the following section.

Other studies that find similar reductions in FA in patients with schizophrenia include Romero et al., 2022, who found reduced FA in the right parahippocampal gyrus and right posterior cingulate cortex in patients with early psychosis [63]. In this study, there is also an observed reduction in average FA in the right parahippocampal gyrus, and effective connections involving the PCC were implicated in two out of four cva models as one of the best predictors of variance in cognitive and clinical scores.

Holleran et al., 2014 found "...that those studies with the largest sample sizes support the case of reduced microstructural organization in the interhemispheric, frontal deep, and temporal WM fibers in schizophrenia, which is consistent with present findings." [38]. Here, bilateral reductions in average FA in the temporal lobes were present, and the frontal paracentral gyrus exhibited reduced average FA in the patient group as well.

Shergill et al., 2007 found "Schizophrenia is associated with altered WM integrity in the tracts connecting the frontal cortex with the temporal and parietal cortices and with contralateral frontal and temporal lobes." [67]. This study identified reductions in average FA across fronto-temporal regions, and also indicated reduced average FA in the left parietal supramarginal gyrus.

Mitelman et al., 2006 found "Overall WM FA was lower in schizophrenic patients than in normal subjects, with regional reductions in widespread temporal parietal and selected prefrontal WM regions", and interestingly, that "...overall WM FA was reduced in patients with poor outcomes in both hemispheres, but to a lesser extent and only in the right hemisphere in patients with good outcomes." [52]. Interestingly, nodes in the left hemisphere were usually involved in connections with the strongest canonical weights in the CVAs that described variance in disease severity via cognitive and clinical scores; namely, those regions are the LiTem, LIns, LlPar_SN, and LaPFC_SN.

For a review that specifically addresses alterations in the occipital cortex in schizophrenia, I direct the reader to Tohid, Faizan, and Faizan, 2015 [75], which makes statements about both structural and functional alterations within the region and its prominent connections.

Overall, the results of this study pertaining to reduced regional fractional anisotropy is consistent with this selection of results present in the literature. More attention to how this may be related to effective connectivity differences that are correlated with varying cognitive deficits and clinical symptom severity will likely be the specific focus of future works.

4.3. Contextualizing the relationship between EC, FA, and altered cognition

In addition to the direct evaluation of differences in EC and FA found between the patient and control groups in this study, the CVA models provide information about how variance in EC strengths correlate with disease severity in the form of cognitive and clinical scores. This section serves to compare the results found in this study to some of the findings that have been reported throughout other studies in the literature. Beginning with Shim et al., 2010 who found "EC decreased from anterior medial prefrontal cortex to LiTem and from PCC to LpCerb, LiTem, and right medial frontal gyrus in schizophrenic patients with auditory

verbal hallucinations." [68]. This thesis indicates the implication of the self-inhibition of the LiTem, the projection from the PCC to the LiTem, and the LpCerb to the RpCerb in the slow 5 CVA model as being the strongest predictors of variance in cognitive scores, specifically with respect to emotion recognition and fluid and crystallized cognition. Furthermore, it is interesting to note that the LiTem is a strong inhibitory source in the schizophrenic group (see Figure 3.8 and Figure 3.9), so a relative self inhibition of the LiTem may disinhibit several target regions potentially resulting in reduced regional dysconnectivity, that is commonly associated with schizophrenia.

Additionally, there are multiple studies that indicate the role of fronto-cingulo connectivity in the processes of memory consolidation of fear conditioning [17], emotional processing [16], and "in mediating cognitive influences on emotion" [73]. Interestingly, in the paper of Feng et al., 2014, the regions that they find implicated in the processes of fear memory consolidation are also the ones most implicated in explaining variance in emotion recognition and fluid and crystallized intelligence in this study; namely, the "...insula, dorsal anterior cingulate, prefrontal cortex, and temporal cortex" [17]. Given that their findings also implicate the amygdala as key mediator within this network, it may be a valuable addition to include in future studies. The alteration of fear memory consolidation in schizophrenia has been studied and evidence in favor of this theory is provided in the following selection of publications: Holt et al., 2009, titled "Extinction memory is impaired in schizophrenia" [39], Pollard et al., 2012 titled "Synaptic transmission changes in fear memory circuits underlie key features of an animal model of schizophrenia" [56], and Clifton et al., 2017 who's "...results suggest that [genomic] copy number variants act to impair inhibitory learning in schizophrenia, potentially contributing to the development of core symptoms of the disorder." [12]. In addition to generally supporting the theory that widespread neuronal dysconnectivity is a feature observable in the brains of people with schizophrenia spectrum disorders, this thesis also provides supporting evidence for the disruption of networks involved in fear memory consolidation, extinction, and emotion regulation being implicated in the severity of symptoms of psychosis.

4.4. Relevance of the findings

The findings of this study are mostly consistent with the findings of the works referred to throughout this chapter. Given that the ROIs and network definitions of the models estimated in those works are different in number and position, the comparisons are not always entirely direct. However, given the overall consistency of the findings of this study with the primary findings of several existing publications, the results of this thesis appear to be sound. As such, this study provides both corroboratory and additive information that may be valuable in advancing the understanding of the neurophysiological mechanisms of early psychosis, specifically in the context of the modernized dysconnectivity hypothesis [21] and with respect to alterations in connectivity within and between the nodes of the triple-network [51]. Furthermore, given that this study is the first of its kind as it investigates EC with a relatively large number of subjects and number of modeled nodes in two distinct

frequency bands, it provides a foundation for asking further research questions related to the dynamics of neurophysiological activities that behave on varying time scales. It may also be interesting to investigate how EC metrics generated using data from distinct frequency bands correlate with regional, select neurotransmitter receptor densities if it would be possible to gain that information via positron emission topography or through the collection of genomic data.

4.5. Limitations of the study

The first limitation of this study is that it is impossible to draw conclusions about nodes that are not modeled in the sp-DCMs, leaving us with an incomplete picture about what overall neurophysiological dynamics look like in a person's brain when they experience psychosis. In the case of estimating fully connected sp-DCM models, the computational cost scales exponentially with each added node, therefore it becomes resource intensive and time consuming to create very large scale models across data sets with many participants. Even with advances in DCM techniques that make the method more computationally efficient [26] [61], it is clear that creating large scale fully connected models over a large number of subjects is expensive and makes results more complicated to interpret. That is the logic that Zarghami et al., 2023 state to explain their decision for using several isolated subnetworks of the brain rather than a fully connected model of 50 nodes, which would yield 2500 connections [86] (See paragraph 17 sentence two of their discussion). Furthermore, given that the number of connections that can be reliably included in CVA models is strongly limited by the number of subjects as was described in section 2.9.1 of this study and in Zarghami et al., 2023 [86], having those additional connections is not necessarily worth the substantial added computational cost of calculating them. The benefit of having a fully connected large-scale model such as the ones used in this study is that it becomes possible to interpret fine grained inter-network node to node connectivity differences and implications in the disorder that cannot be done in non-fully specified models, such as those shown in Zarghami et al., 2023 [86] who state themselves that their between network models were "coarse".

Another limitation of the study is that the number of subjects with schizophrenia and complete cognitive score information was relatively limited as only 45 subjects with schizophrenia were ultimately included in the CVA models. Given that those models have been found to be most reliable when a subject to feature ratio of at least nine is maintained [35] [49] [84][1], having additional subjects would allow for more effective connections or cognitive and clinical features to be interpreted with respect to disease severity.

The final limitations that I am aware of with respect to this study, are that covariates for sex and medication status were not included in the PEB models due to the subsequent added computational cost that arose in the BMR of the fully connected models; and perhaps more concerning, that the control and patient groups were not age matched well with the control group having an average age approximately three years higher than the schizophrenic group.

[1]These studies were referred to in the same capacities in Zarghami et al., 2023 [86]

As a general aside, this study does not consider information that would give a more holistic understanding of how these alterations arise, e.g., genetic information or PET image data. Information about possible alterations in receptor density in the implicated regions and what might cause them would provide added value to this study. These limitations prime some clear, logical extensions for this study and ideas for future studies, that will be commented on in the following section.

4.6. Future works

The first logical extension to this study would be to include the covariates for subject sex and level of medication to the PEB models. Even though they have not been found to statistically significantly affect any individual connections, these variables may moderate the effect of the estimated group differences for given connections, which would be consistent with what Zarghami et al., 2023 found [86] (See paragraph 19 of their discussion). Another reasonable addition to this study would be to isolate the younger group of patients and compare their EC and FA profiles to the older patients to see if there is a trajectory of alteration in either case; and of course, longitudinal studies that include medication naïve subjects would increase our ability to pinpoint those developmental trajectories. This is something that has been called for across existing studies [4] [34] [78][2].

While this study initially aimed to investigate how the interaction between EC and FA might be implicated in various facets of disease severity, the lack of statistical evidence for correlations between FA and EC and between FA and cognitive scores limited the ability to make conclusions about this hypothesized explanatory variable. In a future work, it would be warranted to conduct a systematic review of works that have investigated these relationships, and to better integrate the possible role of FA as a moderator or mediator of the effect of EC on disease severity. This might be done by replicating the methods described in the work of O'muircheartaigh and Jbabdi, 2018 using the HCP-EP dataset, and subsequently using the GM ICs as inputs to the sp-DCMs; this would provide directly coupled FA and EC estimates that would make more streamlined analyses possible.

Another interesting extension would be to train a classification algorithm to use the metrics generated throughout this study to identify the risk for developing schizophrenia and how probable a severe or mild outcome might be via neuroimaging data and EC metrics.

Given access to more computational resources, another logical extension of this study would be to include more nodes in the fully connected DCMs. It would also likely be more sound to utilize ICs to form the basis for selecting the nodes as it was done in the work of Zarghami et al., 2023 [86], rather than using spheres centered around relatively arbitrary positions. Additionally, it could be valuable to integrate other modalities of neuroimaging such as PET, and it would certainly be valuable to gather additional personal information about the subjects e.g., direct information on socioeconomic status and their genotypes in order to better control for factors that may play an important role in the development of psychosis and schizophrenia spectrum disorders.

[2]These studies were referred to in the same capacities in Zarghami et al., 2023 [86]

5. Conclusions

This study's aim is to identify the most salient differences in effective connectivity and fractional anisotropy between healthy controls and patients with schizophrenia spectrum disorders, and to further identify how those metrics might be predictive of disease severity i.e., degree of cognitive deficits and clinical symptom severity. The hypotheses were that there would indeed be distinct differences in EC profiles between the groups, that there would be distributed decreases in regional average FA, and that there would be also be an identifiable association between those metrics and disease severity.

The study successfully identified a relatively broad array of altered EC within and between the DMN, CEN, and SN, and identified regional decreases in average FA that are consistent with other findings in contemporary literature. While this study did not identify a clear relationship between those decreases in FA and disease severity as some others have, it does clearly identify effective connections that are implicated in altered cognitive and clinical scores that are consistent with and add to other findings; those results are summarized at the end of the third chapter.

While this study has its limitations, it still provides information that is novel, corroboratory, and additive to the bodies of literature pertaining to the neurophysiological mechanisms involved in schizophrenia spectrum disorders. Future works will address those limitations and aim to advance the research by means of training classification algorithms. These algorithms would ideally use the most salient information identified in this study and any additional information that can be reliably produced to develop a generalizable tool that is capable of identifying whether an individual is at risk of developing a schizophrenia spectrum disorder, and to what degree they might expect to be affected by it. While there are still hurdles to overcome before reaching that point and realizing any appropriate clinical applications, with advances and investments in computational techniques and resources the techniques used in this thesis may be reasonably employable to aid in the diagnosis and prognosis of schizophrenia and other neurological and psychiatric disorders and diseases.

Acknowledgments

I would like to thank Afra Wohlschläger for guiding and supervising me through this project. I would also like to thank the following members of the lab for their support: Ângelo Bumanglag for executing the minimal preprocessing of the resting state BOLD fMRI data, Yifei Zhang for providing subject-wise 4th ventricle masks that were used to create the CSF signal used in the GLMs of this study, Rachel Nuttall for bringing to our attention that we should be cautious analyzing fractional anisotropy values in an independent component space generated using an unrelated sample, and Fabian Hirsch for being willing to discuss intricacies of the project with me. Finally, I would very much like to thank my family for supporting me while I worked on this thesis.

A. General Addenda

A.1. Regression Tables

The following regression models and respective tables were created using the observed least squares linear modeling tool from python's statsmodels library.

```
                            OLS Regression Results
==============================================================================
Dep. Variable:            comp_aud_HR   R-squared:                       0.183
Model:                            OLS   Adj. R-squared:                  0.172
Method:                 Least Squares   F-statistic:                     16.27
Date:                Mon, 24 Jul 2023   Prob (F-statistic):           4.23e-07
Time:                        16:44:47   Log-Likelihood:                -586.31
No. Observations:                 148   AIC:                             1179.
Df Residuals:                     145   BIC:                             1188.
Df Model:                           2
Covariance Type:            nonrobust
==============================================================================
                 coef    std err          t      P>|t|      [0.025      0.975]
------------------------------------------------------------------------------
const         91.2499      1.832     49.819      0.000      87.630      94.870
sex           -4.5073      2.185     -2.063      0.041      -8.826      -0.188
non_aff      -11.8694      2.135     -5.559      0.000     -16.090      -7.649
==============================================================================
Omnibus:                       50.693   Durbin-Watson:                   1.649
Prob(Omnibus):                  0.000   Jarque-Bera (JB):              110.598
Skew:                          -1.492   Prob(JB):                     9.64e-25
Kurtosis:                       6.005   Cond. No.                         3.26
==============================================================================

Notes:
[1] Standard Errors assume that the covariance matrix of the errors is correctly specified.
```

Figure A.1.: Regression table for composite score of auditory continuous processing test hit rate

OLS Regression Results

Dep. Variable:	comp_aud_RT	R-squared:	0.094
Model:	OLS	Adj. R-squared:	0.081
Method:	Least Squares	F-statistic:	7.499
Date:	Mon, 24 Jul 2023	Prob (F-statistic):	0.000796
Time:	16:44:47	Log-Likelihood:	-884.70
No. Observations:	148	AIC:	1775.
Df Residuals:	145	BIC:	1784.
Df Model:	2		
Covariance Type:	nonrobust		

	coef	std err	t	P>|t|	[0.025	0.975]
const	607.0188	13.755	44.132	0.000	579.833	634.204
sex	34.9394	16.410	2.129	0.035	2.506	67.373
non_aff	56.2303	16.035	3.507	0.001	24.538	87.923

Omnibus:	8.960	Durbin-Watson:	2.165
Prob(Omnibus):	0.011	Jarque-Bera (JB):	9.225
Skew:	0.610	Prob(JB):	0.00993
Kurtosis:	3.074	Cond. No.	3.26

Notes:
[1] Standard Errors assume that the covariance matrix of the errors is correctly specified.

Figure A.2.: Regression table for composite score of auditory continuous processing test response time

```
                            OLS Regression Results
==============================================================================
Dep. Variable:            comp_aud_HR   R-squared:                       0.184
Model:                            OLS   Adj. R-squared:                  0.167
Method:                 Least Squares   F-statistic:                     10.80
Date:                Mon, 24 Jul 2023   Prob (F-statistic):           1.92e-06
Time:                        17:05:52   Log-Likelihood:                -586.27
No. Observations:                 148   AIC:                             1181.
Df Residuals:                     144   BIC:                             1193.
Df Model:                           3
Covariance Type:            nonrobust
============================================================================================
                               coef    std err          t      P>|t|      [0.025      0.975]
--------------------------------------------------------------------------------------------
const                     90.9825      2.090     43.528      0.000      86.851      95.114
sex                       -3.9320      3.066     -1.282      0.202      -9.992       2.128
non_aff                  -11.4066      2.750     -4.148      0.000     -16.842      -5.971
sex_diag_interaction      -1.1772      4.386     -0.268      0.789      -9.846       7.491
==============================================================================
Omnibus:                       50.498   Durbin-Watson:                   1.654
Prob(Omnibus):                  0.000   Jarque-Bera (JB):              110.082
Skew:                          -1.486   Prob(JB):                     1.25e-24
Kurtosis:                       6.003   Cond. No.                         6.50
==============================================================================

Notes:
[1] Standard Errors assume that the covariance matrix of the errors is correctly specified.
```

Figure A.3.: Regression table for composite score of auditory continuous processing test hit rate with interaction term

```
                            OLS Regression Results
==============================================================================
Dep. Variable:            comp_aud_RT   R-squared:                       0.119
Model:                            OLS   Adj. R-squared:                  0.101
Method:                 Least Squares   F-statistic:                     6.489
Date:                Mon, 24 Jul 2023   Prob (F-statistic):           0.000378
Time:                        17:05:52   Log-Likelihood:                -882.60
No. Observations:                 148   AIC:                             1773.
Df Residuals:                     144   BIC:                             1785.
Df Model:                           3
Covariance Type:            nonrobust
===========================================================================================
                              coef    std err          t      P>|t|      [0.025      0.975]
-------------------------------------------------------------------------------------------
const                     622.0351     15.479     40.185      0.000     591.439     652.631
sex                         2.6316     22.705      0.116      0.908     -42.247      47.510
non_aff                    30.2406     20.364      1.485      0.140     -10.011      70.492
sex_diag_interaction       66.1061     32.478      2.035      0.044       1.911     130.301
==============================================================================
Omnibus:                        7.480   Durbin-Watson:                   2.209
Prob(Omnibus):                  0.024   Jarque-Bera (JB):                7.776
Skew:                           0.559   Prob(JB):                       0.0205
Kurtosis:                       2.893   Cond. No.                         6.50
==============================================================================

Notes:
[1] Standard Errors assume that the covariance matrix of the errors is correctly specified.
```

Figure A.4.: Regression table for composite score of auditory continuous processing test response time with interaction term

```
                               OLS Regression Results
==============================================================================
Dep. Variable:     deldisk01_sv_10yr_40000   R-squared:                       0.074
Model:                                 OLS   Adj. R-squared:                  0.061
Method:                      Least Squares   F-statistic:                     5.774
Date:                     Mon, 24 Jul 2023   Prob (F-statistic):            0.00387
Time:                             16:44:47   Log-Likelihood:                -1616.7
No. Observations:                      148   AIC:                             3239.
Df Residuals:                          145   BIC:                             3248.
Df Model:                                2
Covariance Type:                 nonrobust
==============================================================================
                 coef    std err          t      P>|t|      [0.025      0.975]
------------------------------------------------------------------------------
const        1.48e+04   1934.209      7.652      0.000     1.1e+04    1.86e+04
sex        4048.2929   2307.575      1.754      0.081    -512.536    8609.122
non_aff   -5927.4296   2254.845     -2.629      0.009   -1.04e+04   -1470.821
==============================================================================
Omnibus:                       20.215   Durbin-Watson:                   1.802
Prob(Omnibus):                  0.000   Jarque-Bera (JB):               16.459
Skew:                           0.719   Prob(JB):                     0.000267
Kurtosis:                       2.223   Cond. No.                         3.26
==============================================================================

Notes:
[1] Standard Errors assume that the covariance matrix of the errors is correctly specified.
```

Figure A.5.: Regression table for delayed discounting task, $40,000 at a 10 year delay

```
                            OLS Regression Results
==============================================================================
Dep. Variable:     deldisk01_sv_6mo_40000   R-squared:                       0.075
Model:                               OLS   Adj. R-squared:                  0.062
Method:                    Least Squares   F-statistic:                     5.886
Date:                   Mon, 24 Jul 2023   Prob (F-statistic):            0.00349
Time:                           16:44:47   Log-Likelihood:                -1601.5
No. Observations:                    148   AIC:                             3209.
Df Residuals:                        145   BIC:                             3218.
Df Model:                              2
Covariance Type:                nonrobust
==============================================================================
                 coef    std err          t      P>|t|      [0.025      0.975]
------------------------------------------------------------------------------
const       3.348e+04   1745.144     19.182      0.000       3e+04    3.69e+04
sex          -791.4610   2082.015     -0.380      0.704   -4906.479    3323.556
non_aff     -6976.4056   2034.438     -3.429      0.001    -1.1e+04   -2955.421
==============================================================================
Omnibus:                       20.254   Durbin-Watson:                   1.971
Prob(Omnibus):                  0.000   Jarque-Bera (JB):               25.292
Skew:                          -1.013   Prob(JB):                     3.22e-06
Kurtosis:                       2.991   Cond. No.                         3.26
==============================================================================

Notes:
[1] Standard Errors assume that the covariance matrix of the errors is correctly specified.
```

Figure A.6.: Regression table for delayed discounting task, $40,000 at a 6 month delay

```
                                  OLS Regression Results
==============================================================================================================
Dep. Variable:     cogcomp01_nih_fluidcogcomp_unadjusted   R-squared:                       0.294
Model:                                              OLS   Adj. R-squared:                  0.284
Method:                                   Least Squares   F-statistic:                     30.18
Date:                                  Mon, 24 Jul 2023   Prob (F-statistic):           1.10e-11
Time:                                          16:44:47   Log-Likelihood:                -579.83
No. Observations:                                   148   AIC:                             1166.
Df Residuals:                                       145   BIC:                             1175.
Df Model:                                             2
Covariance Type:                               nonrobust
==============================================================================
                 coef    std err          t      P>|t|      [0.025      0.975]
------------------------------------------------------------------------------
const        112.2162      1.753     64.007      0.000     108.751     115.681
sex           -1.1318      2.092     -0.541      0.589      -5.266       3.002
non_aff      -15.8357      2.044     -7.748      0.000     -19.875     -11.796
==============================================================================
Omnibus:                        4.184   Durbin-Watson:                   1.853
Prob(Omnibus):                  0.123   Jarque-Bera (JB):                3.713
Skew:                          -0.369   Prob(JB):                        0.156
Kurtosis:                       3.237   Cond. No.                         3.26
==============================================================================

Notes:
[1] Standard Errors assume that the covariance matrix of the errors is correctly specified.
```

Figure A.7.: Regression table for Fluid Intelligence

OLS Regression Results

Dep. Variable:	cogcomp01_nih_crycogcomp_unadjusted	R-squared:	0.162
Model:	OLS	Adj. R-squared:	0.151
Method:	Least Squares	F-statistic:	14.06
Date:	Mon, 24 Jul 2023	Prob (F-statistic):	2.63e-06
Time:	16:44:47	Log-Likelihood:	-539.68
No. Observations:	148	AIC:	1085.
Df Residuals:	145	BIC:	1094.
Df Model:	2		
Covariance Type:	nonrobust		

	coef	std err	t	P>|t|	[0.025	0.975]
const	110.3325	1.337	82.543	0.000	107.691	112.974
sex	-1.9578	1.595	-1.228	0.222	-5.110	1.194
non_aff	-8.2293	1.558	-5.281	0.000	-11.309	-5.150

Omnibus:	2.152	Durbin-Watson:	1.849
Prob(Omnibus):	0.341	Jarque-Bera (JB):	2.041
Skew:	-0.206	Prob(JB):	0.360
Kurtosis:	2.599	Cond. No.	3.26

Notes:
[1] Standard Errors assume that the covariance matrix of the errors is correctly specified.

Figure A.8.: Regression table for Crystallized Intelligence

OLS Regression Results

Dep. Variable:	er4001_er40_c_cr	R-squared:	0.076
Model:	OLS	Adj. R-squared:	0.063
Method:	Least Squares	F-statistic:	5.949
Date:	Mon, 24 Jul 2023	Prob (F-statistic):	0.00329
Time:	16:44:47	Log-Likelihood:	-377.92
No. Observations:	148	AIC:	761.8
Df Residuals:	145	BIC:	770.8
Df Model:	2		
Covariance Type:	nonrobust		

	coef	std err	t	P>|t|	[0.025	0.975]
const	35.5396	0.448	79.317	0.000	34.654	36.425
sex	0.0208	0.535	0.039	0.969	-1.036	1.077
non_aff	-1.7802	0.522	-3.408	0.001	-2.813	-0.748

Omnibus:	73.707	Durbin-Watson:	1.774
Prob(Omnibus):	0.000	Jarque-Bera (JB):	340.804
Skew:	-1.795	Prob(JB):	9.89e-75
Kurtosis:	9.510	Cond. No.	3.26

Notes:
[1] Standard Errors assume that the covariance matrix of the errors is correctly specified.

Figure A.9.: Regression table for Emotion Recognition, number of correct responses

OLS Regression Results

Dep. Variable:	er4001_er40_c_rtcr	R-squared:	0.183
Model:	OLS	Adj. R-squared:	0.172
Method:	Least Squares	F-statistic:	16.29
Date:	Mon, 24 Jul 2023	Prob (F-statistic):	4.14e-07
Time:	16:44:47	Log-Likelihood:	-1123.3
No. Observations:	148	AIC:	2253.
Df Residuals:	145	BIC:	2262.
Df Model:	2		
Covariance Type:	nonrobust		

	coef	std err	t	P>|t|	[0.025	0.975]
const	1825.2523	68.955	26.470	0.000	1688.965	1961.540
sex	-54.4974	82.266	-0.662	0.509	-217.093	108.098
non_aff	443.4287	80.386	5.516	0.000	284.549	602.308

Omnibus:	66.824	Durbin-Watson:	1.933
Prob(Omnibus):	0.000	Jarque-Bera (JB):	270.198
Skew:	1.652	Prob(JB):	2.12e-59
Kurtosis:	8.735	Cond. No.	3.26

Notes:
[1] Standard Errors assume that the covariance matrix of the errors is correctly specified.

Figure A.10.: Regression table for Emotion Recognition, response time for correct responses

List of Figures

List of Tables

Glossary

Control Executive Network A Fronto-parietal network of brain regions that have been implicated in activating during cognitively challenging tasks, making it a theoretical antagonist to the Default Mode network (DMN). 71

Default Mode Network A network of brain regions implicated in neurophysiological activity patterns associated with not performing any externally demanding tasks. Additionally, it has been found responsible for some "large-scale functional organization" across other networks [58]. 71

Effective Connectivity "effective connectivity describes the causal influences that neural units exert over another [25]". This is a quote from "Analyzing effective connectivity with fMRI", a more recent study that provides more complete details on the definitions of the term [72]. 71

False Discovery Rate "an alternative error criterion representing the expected proportion of false discoveries [of statistically significant test results] among all rejected null hypotheses". (An AI generated note published by Sciencedirect using information from Brain Mapping 2015)[1]. 71

Fractional Anisotropy a metric between 0 and 1 that describes the diffusivity of a volume, where a 0 would represent a purely isotropic volume i.e., one that diffuses freely in any direction equally, and where a 1 would indicate that the volume is strongly restricted and can only move along one axis. Practically, values close to 1 imply high densities of white matter and values close to 0 imply low white matter densities in this context. 71

Grey Matter Generally, unmyelinated neurons. 72

Positive and Negative Syndrome Scale Scale for measuring the severity of positive and negative symptoms in schizophrenia; first published by Stanley Kay, Abraham Fiszbenm and Lewis Opler in 1987 [45]. 72

Salience Network "a large-scale para-limbic network anchored in the anterior insula and dorsal Anterior Cingulate Cortex (dACC) with prominent subcortical nodes in affect and reward processing systems" (An AI generated note published by Sciencedirect using information from Brain Mapping, 2015)[2] . 73

[1] https://www.sciencedirect.com/topics/neuroscience/false-discovery-rate

[2] `https://www.sciencedirect.com/topics/psychology/salience-network`

White Matter Generally, myelinated neurons. 73

Acronyms

acpt Seidmann auditory continous performance test. 16, 32

AP Anterior-Posterior. 2, 7, 11

BEDPOSTX Bayesian Estimation of Diffusion Parameters using Sampling Techniques. 12

BMR Bayesian Model Reduction. iv, 9, 10, 16–19, 48, 54, 65

BOLD Blood Oxygen Level Dependent. iv, 1, 2, 6, 7

CEN Control Executive Network. 1, 3, 4, 20, 22–25, 48, 49, 56, 65

CSF Cerebro-Spinal Fluid. 8

CVA Canonical Variate Analysis. iv, 14–16, 35, 50–54

dACC dorsal Anterior Cingulate Cortex. 4, 35, 49, 50, 69

DCM Dynamic Causal Model. 50, 54, 55

DCT Discrete Cosine Transform. 8

DMN Default Mode network. 1, 3, 4, 20, 22–25, 48, 49, 51, 56, 65, 69

dmPFC dorsal medial Prefrontal Cortex. 4, 35, 49

dMRI Diffusion Magnetic Resonance Imaging. 2, 11

DWI Diffusion Weighted Image. 1

EC Effective Connectivity. iv, v, 1, 5, 6, 9–11, 15–17, 20, 22–25, 27–31, 35, 36, 39, 42, 45, 48, 50–56, 65, 66

FA Fractional Anisotropy. iv, v, 1, 5, 6, 12–14, 16, 31, 32, 35, 48, 50–52, 55, 56

FDR False Discovery Rate. 14, 16, 31, 48

fMRI Functional Magnetic Resonance Imaging. iv, 1, 2, 6, 7, 15

FSL FMRIB Software Library. 6, 7, 11–13

FWHM Full width half maximum. 7

GLM General Linear Model. 7

GLMs General Linear Models. 7

GM Grey Matter. 31, 55

GPU Graphics Processing Unit. 12

HCP Human Connectome Project. 11

HCP-EP Human Connectome Project for Early Psychosis. 2, 6, 33, 55

IC Independent Component. 12–14, 16, 31, 48, 55

ICA Independent Component Analysis. 13

LaPFC Left anterior Prefrontal Cortex (Inferior, Brodmann area 45). 4

LaPFC_SN Left anterior Prefrontal Cortex of the Salience Network (Superior Frontal Gyrus). 4, 26, 35, 48, 49, 52

LIns Left Insula. 4, 26, 35, 48, 51, 52

LiTem Left inferior Temporal Cortex. 4, 35, 48, 51–53

LlPar Left lateral Parietal Cortex (Angular Gyrus). 4

LlPar_SN Left lateral Parietal Cortex of the Salience Network (Supramarginal Gyrus). 4, 35, 48, 52

LpCerb Left posterior Cerebellum. 4, 35, 48, 52, 53

LsPar Left superior Parietal Cortex. 4

mdThal medial dorsal Thalamus. 4, 35, 49

mPFC medial Prefrontal Cortex. 4, 35, 49, 50

NIH-CB NIH Toolbox Cognitive Battery. 34

PA Posterior-Anterior. 2, 7, 11

PANSS Positive and Negative Syndrome Scale. 2, 15, 16, 35, 49, 50

PCA Principal Component Analysis. 11, 13

PCC Posterior Cingulate Cortex. 4, 35, 48, 51–53

PEB Parametric Empirical Bayes. iv, 9, 10, 16, 17, 48, 54, 55

RaPFC Right anterior Prefrontal Cortex (Inferior, Brodmann area 45). 4

RaPFC_SN Right anterior Prefrontal Cortex of the Salience Network (Superior Frontal Gyrus). 4

RIns Right Insula. 4, 26

RiTem Right inferior Temporal Cortex. 4, 35, 49

RlPar Right lateral Parietal Cortex (Angular Gyrus). 4, 35, 48, 49, 51

RlPar_SN Right lateral Parietal Cortex of the Salience Network (Supramarginal Gyrus). 4, 26, 35, 49

ROI Region of Interest. 4, 8, 13, 68

ROIs Regions of Interest. 1, 3, 5, 9, 12, 14, 16, 31, 53

RpCerb Right posterior Cerebellum. 4, 35, 48, 53

rs-fMRI resting state fMRI. 7

RsPar Right superior Parietal Cortex. 4

SN Salience Network. 1, 3, 4, 20, 22–25, 48, 56, 65

sp-DCM Spectral Dynamic Causal Model. 8, 9, 16, 31, 51, 54, 55

spDCMs Spectral Dynamic Causal Models. 1

SPM Statistical Parametric Mapping. 7–9, 14

TR Repetition Time. 2

WM White Matter. 5, 12, 31, 48, 51, 52

Bibliography

1. Andersson, J. L. R. *et al.* Incorporating outlier detection and replacement into a non-parametric framework for movement and distortion correction of diffusion MR images. *Neuroimage* (2016).
2. Andersson, J. L. R., Skare, S. & Ashburner, J. How to correct susceptibility distortions in spin-echo echo-planar images: application to diffusion tensor imaging. *Neuroimage* (2003).
3. Andersson, J. L. R. & Sotiropoulos, S. N. An integrated approach to correction for off-resonance effects and subject movement in diffusion MR imaging. *Neuroimage* (2016).
4. Anticevic, A., Hu, X., Xiao, Y., Hu, J., Li, F., Bi, F., Cole, M. W., Savic, A., Yang, G. J., Repovs, G., *et al.* Early-course unmedicated schizophrenia patients exhibit elevated prefrontal connectivity associated with longitudinal change. *Journal of Neuroscience* **35,** 267–286 (2015).
5. Arciniegas, D. B. Psychosis. *Continuum: Lifelong Learning in Neurology* **21,** 715 (2015).
6. Ardekani, B. A., Nierenberg, J., Hoptman, M. J., Javitt, D. C. & Lim, K. O. MRI study of white matter diffusion anisotropy in schizophrenia. *Neuroreport* **14,** 2025–2029 (2003).
7. Bastiani, M. *et al.* Automated quality control for within and between studies diffusion MRI data using a non-parametric framework for movement and distortion correction. *Neuroimage* (2019).
8. Bautista, T., O'Muircheartaigh, J., Hajnal, J. V. & Tournier, J.-D. Removal of Gibbs ringing artefacts for 3D acquisitions using subvoxel shifts. *Proc. ISMRM* (2021).
9. Behrens, T. E. J. *et al.* Characterization and propagation of uncertainty in diffusion-weighted MR imaging. *Magnetic Resonance in Medicine* (2003).
10. Benjamini, Y. & Hochberg, Y. Controlling the False Discovery Rate: A Practical and Powerful Approach to Multiple Testing. *Journal of the Royal Statistical Society: Series B (Methodological)* (1995).
11. Bumanglag, Â. A. Brain Dynamics in Relation to Activity of the Ventral Tegmental Area in Young Patients with Schizophrenia Studied by Resting State FMRI (2023).
12. Clifton, N., Pocklington, A., Scholz, B., Rees, E., Walters, J., Kirov, G., O'Donovan, M., Owen, M., Wilkinson, L., Thomas, K., *et al.* Schizophrenia copy number variants and associative learning. *Molecular psychiatry* **22,** 178–182 (2017).
13. Cordero-Grande, L. *et al.* Complex diffusion-weighted image estimation via matrix recover under general noise models. *Neuroimage* (2019).

14. Csukly, G. *et al.* Fronto-thalamic structural and effective connectivity and delusions in schizophrenia: a combined DTI/DCM study. *Psychological Medicine* (2020).
15. Deserno, L., Sterzer, P., Wüstenberg, T., Heinz, A. & Schlagenhauf, F. Reduced prefrontal-parietal effective connectivity and working memory deficits in schizophrenia. *Journal of Neuroscience* **32,** 12–20 (2012).
16. Etkin, A., Egner, T. & Kalisch, R. Emotional processing in anterior cingulate and medial prefrontal cortex. *Trends in cognitive sciences* **15,** 85–93 (2011).
17. Feng, P., Feng, T., Chen, Z. & Lei, X. Memory consolidation of fear conditioning: bi-stable amygdala connectivity with dorsal anterior cingulate and medial prefrontal cortex. *Social cognitive and affective neuroscience* **9,** 1730–1737 (2014).
18. Fischl, B. FreeSurfer. *Neuroimage* **62,** 774–781 (2012).
19. Friston, K. Learning and inference in the brain. *Neural Networks* **16,** 1325–1352 (2003).
20. Friston, K. *et al.* Variational free energy and the Laplace approximation. *Neuroimage* (2007).
21. Friston, K., Brown, H. R., Siemerkus, J. & Stephan, K. E. The dysconnection hypothesis (2016). *Schizophrenia research* **176,** 83–94 (2016).
22. Friston, K., Parr, T. & Zeidman, P. Bayesian model reduction. *arXiv preprint arXiv:1805.07092* (2018).
23. Friston, K., Zeidman, P. & Litvak, V. Empirical Bayes for DCM: a group inversion scheme. *Frontiers in systems neuroscience* **9,** 164 (2015).
24. Friston, K. J. *et al.* Bayesian model reduction and empirical Bayes for group (DCM) studies. *Neuroimage* (2016).
25. Friston, K. J. Functional and effective connectivity in neuroimaging: a synthesis. *Human brain mapping* **2,** 56–78 (1994).
26. Friston, K. J. *et al.* A DCM for resting state fMRI. *NeuroImage* (2014).
27. Friston, K. J. *et al.* On nodes and modes in resting state fMRI. *Neuroimage* (2014).
28. Gelman, A., Hill, J. & Yajima, M. Why we (usually) don't have to worry about multiple comparisons. *Journal of research on educational effectiveness* **5,** 189–211 (2012).
29. Gelman, A. & Tuerlinckx, F. Type S error rates for classical and Bayesian single and multiple comparison procedures. *Computational statistics* **15,** 373–390 (2000).
30. Glasser, M. F. *et al.* The minimal preprocessing pipelines for the Human Connectome Project. *Neuroimage* (2013).
31. Graham, M. S., Drobnjak, I., Jenkinson, M. & Zhang, H. Quantitative assessment of the susceptibility artefact and its interaction with motion in diffusion MRI. *PLoS One* (2017).
32. Gur, R. C. A cognitive neuroscience-based computerized battery for efficient measurement of individual differences: standardization and initial construct validation. *Journal of Neuroscience Methods* (2010).

33. Gur, R. C. *et al.* Computerized neurocognitive scanning: II. The profile of schizophrenia. *Neuropsychopharmacology* (2001).

34. Hadley, J. A., Kraguljac, N. V., White, D. M., Ver Hoef, L., Tabora, J. & Lahti, A. C. Change in brain network topology as a function of treatment response in schizophrenia: a longitudinal resting-state fMRI study using graph theory. *npj Schizophrenia* **2,** 1–7 (2016).

35. Helmer, M. *et al.* On stability of Canonical Correlation Analysis and Partial Least Squares with application to brain-behavior associations. *bioRxiv* (2020).

36. Hernández, M. *et al.* Accelerating Fibre Orientation Estimation from Diffusion Weighted Magnetic Resonance Imaging Using GPUs. *PloS One* (2013).

37. Hodes, R. J. *et al.* The NIH toolbox, setting a standard for biomedical research. *Neurology* (2013).

38. Holleran, L., Ahmed, M., Anderson-Schmidt, H., McFarland, J., Emsell, L., Leemans, A., Scanlon, C., Dockery, P., McCarthy, P., Barker, G. J., *et al.* Altered interhemispheric and temporal lobe white matter microstructural organization in severe chronic schizophrenia. *Neuropsychopharmacology* **39,** 944–954 (2014).

39. Holt, D. J., Lebron-Milad, K., Milad, M. R., Rauch, S. L., Pitman, R. K., Orr, S. P., Cassidy, B. S., Walsh, J. P. & Goff, D. C. Extinction memory is impaired in schizophrenia. *Biological psychiatry* **65,** 455–463 (2009).

40. Jbabdi, S. *et al.* Model-based analysis of multishell diffusion MR data for tractography: how to get over fitting problems (2012).

41. Jbabdi, S. *et al.* Model-based analysis of multishell diffusion MR data for tractography: how to get over fitting problems. *Magnetic Resonance in Medicine* (2012).

42. Jbabdi, S. & Johansen-Berg, H. Tractography: where do we go from here? *Brain connectivity* **1,** 169–183 (2011).

43. Jenkinson, M. *et al.* FSL. *Neuroimage* (2012).

44. Jenkinson, M. *et al.* Improved optimization for the robust and accurate linear registration and motion correction of brain images. *Neuroimage* (2002).

45. Kay, S., Fiszbein, A. & Opler, L. The Positive and Negative Syndrome Scale (PANSS) for schizophrenia. *Schizophrenia Bulletin* (1987).

46. Kellner, E., Dhital, B., Kiselev, V. G. & Reisert, M. Gibbs-ringing artifact removal based on local subvoxel-shifts. *Magnetic Resonance in Medicine* (2016).

47. Lancaster, J. L. *et al.* Automated Talairach atlas labels for functional brain mapping. *Human Brain Mapping* (2000).

48. Lancaster, J. L. *et al.* Bias between MNI and Talairach coordinates analyzed using the ICBM-152 brain template. *Human Brain Mapping* (2007).

49. Leach, L. F. & Henson, R. K. Bias and Precision of the Squared CanonicalCorrelation Coefficient Under Nonnormal DataCondition. *Journal of Modern Applied Statistical Methods* (2014).
50. Lim, K. O., Hedehus, M., Moseley, M., De Crespigny, A., Sullivan, E. V. & Pfefferbaum, A. Compromised white matter tract integrity in schizophrenia inferred from diffusion tensor imaging. *Archives of general psychiatry* **56,** 367–374 (1999).
51. Menon, V. Large-scale brain networks and psychopathology: a unifying triple network model. *Trends in cognitive sciences* **15,** 483–506 (2011).
52. Mitelman, S. A., Newmark, R. E., Torosjan, Y., Chu, K.-W., Brickman, A. M., Haznedar, M. M., Hazlett, E. A., Tang, C. Y., Shihabuddin, L. & Buchsbaum, M. S. White matter fractional anisotropy and outcome in schizophrenia. *Schizophrenia research* **87,** 138–159 (2006).
53. Neath, A. A., Flores, J. E. & Cavanaugh, J. E. Bayesian multiple comparisons and model selection. *Wiley Interdisciplinary Reviews: Computational Statistics* **10,** e1420 (2018).
54. O'muircheartaigh, J. & Jbabdi, S. Concurrent white matter bundles and grey matter networks using independent component analysis. *Neuroimage* (2018).
55. Parkes, L. *et al.* An evaluation of the efficacy, reliability, and sensitivity of motion correction strategies for resting-state functional MRI. *Neuroimage* (2018).
56. Pollard, M., Varin, C., Hrupka, B., Pemberton, D. J., Steckler, T. & Shaban, H. Synaptic transmission changes in fear memory circuits underlie key features of an animal model of schizophrenia. *Behavioural brain research* **227,** 184–193 (2012).
57. Rahman, T. & Lauriello, J. Schizophrenia: an overview. *Focus* **14,** 300–307 (2016).
58. Raichle, M. E. The brain's default mode network. *Annual Review Neuroscience* (2015).
59. Raichle, M. E. The Restless Brain. *Brain Connectivity* (2011).
60. Razi, A. *et al.* Construct validation of a DCM for resting state fMRI. *Neuroimage* (2015).
61. Razi, A. *et al.* Large-scale DCMs for resting-state fMRI. *Network Neuroscience* (2017).
62. Rihs, T. A., Tomescu, M. I., Britz, J., Rochas, V., Custo, A., Schneider, M., Debbané, M., Eliez, S. & Michel, C. M. Altered auditory processing in frontal and left temporal cortex in 22q11. 2 deletion syndrome: a group at high genetic risk for schizophrenia. *Psychiatry Research: Neuroimaging* **212,** 141–149 (2013).
63. Romero, S., de la Serna, E., Baeza, I., Valli, I., Pariente, J. C., Picado, M., Bargalló, N., Sugranyes, G. & Castro-Fornieles, J. Altered White Matter Integrity at Illness Onset in Adolescents With a First Episode of Psychosis. *Frontiers in Psychiatry* **13,** 876793 (2022).
64. Seghier, M. L. & Friston, K. J. Network discovery with large DCMs. *Neuroimage* **68,** 181–191 (2013).
65. Seidman, L. J. *et al.* Auditory working memory impairments in individuals at familial high risk for schizophrenia. *Neuropsychology* (2012).

66. Seidmann, L. J. *et al.* A functional magnetic resonance imaging study of auditory vigilance with low and high information processing demands. *Neuropsychology* (1998).

67. Shergill, S. S., Kanaan, R. A., Chitnis, X. A., O'Daly, O., Jones, D. K., Frangou, S., Williams, S. C., Howard, R. J., Barker, G. J., Murray, R. M., *et al.* A diffusion tensor imaging study of fasciculi in schizophrenia. *American Journal of Psychiatry* **164,** 467–473 (2007).

68. Shim, G., Oh, J. S., Jung, W. H., Jang, J. H., Choi, C.-H., Kim, E., Park, H.-Y., Choi, J.-S., Jung, M. H. & Kwon, J. S. Altered resting-state connectivity in subjects at ultra-high risk for psychosis: an fMRI study. *Behavioral and Brain Functions* **6,** 1–11 (2010).

69. Sizemore, A. E. & Bassett, D. S. Dynamic graph metrics: Tutorial, toolbox, and tale. *NeuroImage* **180,** 417–427 (2018).

70. Smith, S. M. *et al.* Advances in functional and structural MR image analysis and implementation as FSL. *Neuroimage* (2004).

71. Smith, S. M., Hyvärinen, A., Varoquaux, G., Miller, K. L. & Beckmann, C. F. Group-PCA for very large fMRI datasets. *Neuroimage* **101,** 738–749 (2014).

72. Stephan, K. E. & Friston, K. J. Analyzing effective connectivity with functional magnetic resonance imaging. *Wiley Interdisciplinary Reviews: Cognitive Science* **1,** 446–459 (2010).

73. Stevens, F. L., Hurley, R. A. & Taber, K. H. Anterior cingulate cortex: unique role in cognition and emotion. *The Journal of neuropsychiatry and clinical neurosciences* **23,** 121–125 (2011).

74. Talairach, J. & Tournoux, P. Co-planar stereotaxic atlas of the human brain: 3-Dimensional proportional system: An approach to cerebral imaging. *Thieme Medical Publishers Inc., New York* (1988).

75. Tohid, H., Faizan, M. & Faizan, U. Alterations of the occipital lobe in schizophrenia. *Neurosciences Journal* **20,** 213–224 (2015).

76. Tong, Y. *et al.* Perfusion information extracted from resting state functional magnetic resonance imaging. *Journal of Cerebral Blood Flow & Metabolism* (2017).

77. Tournier, J.-D. *et al.* MRtrix3: a fast, flexible, and open software framework for medial image processing and visualization. *Neuroimage* (2019).

78. Towlson, E. K., Vértes, P. E., Müller-Sedgwick, U. & Ahnert, S. E. Brain networks reveal the effects of antipsychotic drugs on schizophrenia patients and controls. *Frontiers in Psychiatry* **10,** 611 (2019).

79. Veraart, J. *et al.* Denoising of diffusion MRI using random matrix theory. *Neuroimage* (2016).

80. Veraart, J., Fieremans, E. & Novikov, D. S. Diffusion MRI noise mapping using random matrix theory. *Magnetic Resonance in Medicine* (2016).

81. Weintraub, S. *et al.* I. NIH Toolbox Cognition Battery (CB): introduction and pediatric data. *Monographs of the Society for Research in Child Development* (2013).

82. Weintraub, S. *et al.* The cognition battery of the NIH toolbox for assessment of neurological and behavioral function: validation in an adult sample. *Journal of the International Neuropsychology Society* (2014).

83. Yan, C.-G., Wang, X.-D., Zuo, X.-N. & Zang, Y.-F. DPABI: data processing & analysis for (resting-state) brain imaging. *Neuroinformatics* **14,** 339–351 (2016).

84. Yang, Q. *et al.* Stability test of canonical correlation analysis for studying brain-behavior relationships: The effects of subject-to-variable ratios and correlation strengths. *Human Brain Mapping* (2021).

85. Yao, L., Lui, S., Liao, Y., Du, M.-Y., Hu, N., Thomas, J. A. & Gong, Q.-Y. White matter deficits in first episode schizophrenia: an activation likelihood estimation meta-analysis. *Progress in Neuro-Psychopharmacology and Biological Psychiatry* **45,** 100–106 (2013).

86. Zarghami, T. S. *et al.* Dysconnection and cognition in schizophrenia: A spectral dynamic causal modeling study. *Human Brain Mapping* (2023).

87. Zeidman, P., Jafarian, A., Seghier, M. L., Litvak, V., Cagnan, H., Price, C. J. & Friston, K. J. A guide to group effective connectivity analysis, part 2: Second level analysis with PEB. *Neuroimage* **200,** 12–25 (2019).

88. Zelazo, P. D. *et al.* II. NIH Toolbox Cognition Battery (CB): measuring executive function and attention. *Monographs of the Society for Research in Child Development* (2013).

89. Zhou, Y. *et al.* Altered intrinsic and extrinsic connectivity in schizophrenia. *NeuroImage: Clinical* (2018).